

Migration barriers for diffusion of As and P atoms in InP and InAs via vacancies and interstitial atoms

Ivan A. Aleksandrov, Konstantin S. Zhuravlev

Rzhanov Institute of Semiconductor Physics, Siberian Branch of Russian Academy of Sciences, Novosibirsk, Russia

Abstract

Processes of diffusion of As and P atoms in InP and InAs, and atomic and energy structure of group-V vacancies and interstitial P and As atoms in InP and InAs have been investigated using density functional theory. Formation energies of group-V vacancies in InP and InAs and P and As interstitial atoms in InP and InAs have been calculated with hybrid functional. The main types of migration jumps have been determined, and the energy favorable migration paths and migration barriers of As and P atoms diffusion in InP and InAs via vacancies and interstitial atoms have been calculated using climbing image nudged elastic band method. In the case of diffusion of As and P atoms in InP and InAs via interstitial atoms the diffusion process occurs via indirect interstitial mechanism. The migration energy barriers for the vacancy diffusion mechanism are 1.5–2.0 eV, the migration energy barriers for the interstitialcy mechanism are 0.3–0.6 eV. The interstitial atoms have higher formation energies compared to the formation energies of the vacancies, and total activation energies of the diffusion are comparable for the vacancy and interstitialcy mechanisms. The obtained results will be useful for modeling of the diffusion processes in semiconductor structures based on InP and InAs.

Keywords:

diffusion, InP, InAs, density functional theory, hybrid functional, vacancy, interstitial atom, vacancy mechanism, interstitialcy mechanism, dumbbell interstitial, split-interstitial, correlation factor, zinc-blende structure

1. Introduction

Heterostructures based on A_3B_5 compounds on InP substrates are promising for creating of optoelectronic devices in the spectral range of 1.3–1.6 μm : semiconductor lasers [1, 2], photodetectors [3, 4], single photon sources [5], as well as for the creation of field-effect and bipolar transistors [6] and photonic integrated circuits [7].

Atomic diffusion is a fundamentally important process for the manufacturing technology of the semiconductor structures. Diffusion of atoms at the material interfaces and diffusion of dopants is one of the limiting factors for reducing the size of nanoelectronic devices. The diffusion of atoms in heterostructures affects the sharpness of the composition profile at the heterointerfaces, so it must be taken into account during the calculations of the parameters of the device structures and when choosing modes for the growth of heterostructures and for the manufacture of devices. Modification of the composition profile at heterointerfaces affects the energies of optical transitions and radiative lifetimes in heterostructures [8, 9]. Controlled annealing of structures with quantum wells can be used to intentionally change the energies of optical transitions [1].

To theoretically describe the diffusion processes, various continuum models are used [10, 11, 12], as well as kinetic Monte Carlo models [13, 14] and molecular dynamics [15, 16]. The key parameters of continuum and Monte Carlo models

are the energy barriers of the atomic diffusion, and the formation energies of defects involved in the diffusion process, which determine their concentration for the equilibrium case. To determine these parameters, fitting of experimental results and ab initio calculations [17] are used. Calculation of these parameters using density functional theory is useful in that it allows one to obtain a theoretically based estimate of these parameters, and obtain information about the most probable types of atomic transitions that determine the microscopic diffusion mechanism. Among the A_3B_5 compounds with sphalerite structure, diffusion processes have been most studied in gallium arsenide [18, 19, 20, 21]. Calculations of the migration energy barriers are known for Ga and As vacancies in GaAs [18, 22], interstitial Ga atoms [19, 23] and interstitial As atoms [20, 21] in GaAs, and silicon atoms in GaAs [24]. Diffusion processes in InP and InAs have been less studied theoretically. There are known calculations of the energy structure of defects in InP [25, 26, 27, 28], calculations of migration barriers of Zn diffusion in InP [29], neutral intrinsic defects and silicon in InAs [30], and silicon atoms in InGaAs [31]. We conclude that for such fundamentally important processes as the self-diffusion of P in InP and As in InAs and the diffusion of As in InP and P in InAs, the theoretical calculation of energy barriers of diffusion and migration paths is an actual task.

In this work, calculations of the migration energy barriers and migration paths for the diffusion of As and P atoms in InP and InAs via vacancies and interstitial atoms, formation energies of phosphorus vacancies in InP, arsenic vacancies in InAs

Email address: aleksandrov@isp.nsc.ru (Ivan A. Aleksandrov)

and interstitial As and P atoms in InP and InAs have been carried out. Activation energies and pre-exponential factors for the diffusion coefficients of As and P in InP and InAs have been estimated. The calculation results are compared with the experimental data available in the literature.

2. Calculation details

2.1. Details of DFT calculations of atomic structure and formation energies of defects and migration energy barriers for As and P in InAs and InP

Calculations of the atomic structure and formation energies of vacancies and interstitial atoms in InP and InAs were carried out using density functional theory in the Quantum ESPRESSO software package [32, 33] for supercells corresponding to 64 and 216 lattice sites of bulk InP and InAs. Calculations of defect formation energies were carried out using the hybrid HSE functional [34, 35] with 64-site supercells and the generalized gradient approximation with the PBE functional [36] with 64- and 216-site supercells for convergence checking. Calculations with the hybrid functional were carried out with a standard value of the Hartree-Fock exchange fraction $\alpha=0.25$, which gives the values of the band gap of InP $E_g=1.419$ eV and InAs $E_g=0.507$ eV, which are consistent with the experiment for InP $E_g=1.424$ eV [37] and InAs $E_g=0.417$ eV [37]. For the calculations with the PBE functional we used optimized norm-conserving Vanderbilt pseudopotentials [38, 39]. For calculations with the hybrid HSE functional, pseudopotentials of the same type were used, but generated without nonlinear core correction using the ONCVSP code [38]. The cutoff energy for the wave functions was 80 Ry, which gives total energy convergence of 0.3 meV/atom in the case of the PBE functional and 4 meV/atom in the case of the HSE functional. For defect calculations, a $2 \times 2 \times 2$ k-point mesh was used, shifted by half a grid step relative to the Gamma point along each coordinate, which gives total energy convergence of 1 meV/atom. The following convergence criteria were used for relaxation of the atomic structure: 10^{-5} Ry for total energy and 10^{-4} eV/Å for forces. Spin polarization was taken into account in the collinear approximation. To take into account the interaction of supercells with charged defects, the total energy was corrected using the method proposed in [40, 41], with the experimental values of the dielectric constants of InP $\epsilon=12.55$ [42] and InAs $\epsilon=15.15$ [43]. Formation energies of the defects were calculated using the expression: [44, 45]:

$$E_{form}^{def}(q) = E_{tot}^{def}(q) - E_{tot}^{bulk} - \sum_i n_i \mu_i + q(E_f + E_v), \quad (1)$$

where $E_{form}^{def}(q)$ is the formation energy of the defect in the charge state q , $E_{tot}^{def}(q)$ is total energy of a supercell with a defect, E_{tot}^{bulk} is total energy of a perfect bulk supercell, n_i is number of atoms of i -th element added ($n_i > 0$) or removed ($n_i < 0$) from the supercell with the defect, μ_i is a chemical potential of the corresponding element, E_v is the valence band edge of the bulk material, and E_f is the Fermi level counted from the

valence band edge. The limiting phases for the chemical potentials in the calculation of formation energies were: bulk metallic indium with bcc tetragonal structure, bulk black phosphorous, bulk gray arsenic, bulk InP for chemical potential of P impurity in InAs and bulk InAs for chemical potential of As impurity in InP.

Migration energy barriers and migration paths were calculated using climbing image nudged elastic band method (CI NEB) [46] with the PBE functional for 64-site supercells. We have checked convergence of the migration barrier value with the supercell size for neutral P_i in InP using 217-atom supercell. The migration barrier increases by 0.016 eV from 0.396 eV for 65-atom supercell to 0.412 eV for 217-atom supercell. Spin polarization was supposed to be unchanged during migration transitions.

InP lattice parameter, calculated with the PBE and HSE functionals, is $a=5.959$ Å and $a=5.854$ Å, respectively, which differs by 1.5% and 0.3% from the experimental value $a=5.870$ Å [37]. For InAs, the calculated lattice parameter is $a=6.171$ Å and $a=6.032$ Å, for the PBE and HSE functionals, respectively, which differs by 1.9% and 0.4% from the experimental value $a=6.058$ Å [37]. Enthalpy of InP formation relative to bcc tetragonal indium and black phosphorous calculated with the PBE functional is -0.477 eV, and with the HSE functional is -0.653 eV. Enthalpy of InAs formation is -0.461 eV for the PBE functional and -0.769 eV for the HSE functional. These values are consistent within 0.17 eV with the experimental values -0.499 eV for InP [47] and -0.622 eV for InAs [48].

Concentration of defects can be calculated from the expression [45]:

$$N_{def} = N_{sites} \exp\left(-\frac{G_{form}}{k_B T}\right), \quad (2)$$

where N_{def} is the number of defects per unit volume, N_{sites} is the number of the lattice sites per unit volume, G_{form} is the Gibbs energy of defect formation: $G_{form} = H_{form} - TS_{form}$, where $H_{form} = E_{form} + PV_{form}$ is the enthalpy of defect formation, V_{form} is the volume of defect formation, and S_{form} is the entropy of defect formation. Expression 1 for the formation energy is valid in the limit of low temperatures. More accurate methods are known for calculation of defect concentrations at finite temperatures, which take into account vibrational and electronic excited states [45, 49, 50]. Vibrational excitations can be considered in the quasi-harmonic approximation or taking into account anharmonicity. The assumption of a close to the equilibrium concentration of defects is fulfilled only for certain experimental conditions (sufficiently high temperatures and close to equilibrium vapor pressures). At relatively low temperatures, a “frozen” concentration of defects can often be observed, which is higher than the equilibrium concentration [51].

2.2. Calculation of diffusion coefficients of As and P atoms in InP and InAs

Diffusion coefficient of atoms for one type of the jumps can be calculated as [52, 53]:

$$D = \frac{1}{6} r^2 \Gamma f, \quad (3)$$

where r is the jump distance, Γ is the number of jumps per unit time, f is the correlation coefficient. For vacancy mechanism of diffusion the jump frequency Γ can be found as [53]: $\Gamma = Z \frac{N_{def}}{N_{sites}} w$, where Z is the number of the nearest neighbor places for the jump, N_{def} is the number of defects per unit volume, N_{sites} is the number of lattice sites per unit volume, w is jump probability per unit time in one direction. Diffusion coefficient of vacancies is expressed as:

$$D = \frac{1}{6} r^2 Z w. \quad (4)$$

Jump frequency w can be found as [54, 55] $w = \tilde{\nu} \exp\left(\frac{S_m}{k_B T}\right) \exp\left(-\frac{H_m}{k_B T}\right) = \nu^* \exp\left(-\frac{H_m}{k_B T}\right)$, where $\tilde{\nu}$ is the frequency of vibrational mode in the jump direction, H_m is the enthalpy of migration, S_m is the entropy of migration. In further calculations we do not take into account the migration entropy and migration volume and assume that $w = \nu \exp\left(-\frac{E_m}{k_B T}\right)$, where E_m is migration barrier energy of the atom and ν is attempt frequency. The frequency of vibrational mode in the jump direction can be approximately calculated as the Einstein frequency of the moving atom in the jump direction [55]. We used this method in our earlier work [56]. In this work depending on the transition type we took into account one, two or three atoms with largest displacements. The frequency ν was calculated as $\frac{1}{2\pi} \sqrt{\frac{K}{M}}$, the effective mass M of the vibrational mode was calculated as $M = \frac{\sum_a r_a^2 m_a}{\sum_a r_a^2}$, where r_a and m_a are displacement and mass of the atom a , force constant K was determined from the expression $E = \frac{K}{2} \sum_a r_a^2$ for several points of the dependence of the energy on the displacements of the considered atoms along the migration path near the equilibrium position.

For self-diffusion of atoms in group-V elements sublattice by vacancy mechanism we have used the correlation coefficient, calculated by Compaan and Haven [57] for fcc lattice $f=0.78146$. For diffusion of As atoms in InP and P atoms in InAs by vacancy mechanism the correlation factors were calculated by Manning expression [58], obtained in the five-frequency model for fcc lattice:

$$f = \frac{w_1 + 7F_3 w_3 / 2}{w_2 + w_1 + 7F_3 w_3 / 2}, \quad (5)$$

$$7F_3(\alpha) = 7 - \frac{10\alpha^4 + 180.5\alpha^3 + 927\alpha^2 + 1341\alpha}{2\alpha^4 + 40.2\alpha^3 + 254\alpha^2 + 597\alpha + 436}, \quad (6)$$

where w_1 is the jump rate of the vacancy between first-nearest neighbor sites of the impurity atom in the group-V sublattice, w_2 is the jump rate of the vacancy to the impurity atom site, w_3 is the jump rate of the vacancy from first coordination shell of the impurity atom to second coordination shell in the group-V sublattice, w_4 is the jump rate of the reverse of a w_3 jump, w_0 is the jump rate of all other jumps in the group-V sublattice, $\alpha = \frac{w_4}{w_0}$. We assume that $w_1 = w_0 = \nu_{bulk} \exp\left(-\frac{E_{mbulk}}{k_B T}\right)$, $w_2 = \nu \exp\left(-\frac{E_m}{k_B T}\right)$, $w_3 = \nu_{bulk} \exp\left(-\frac{E_{mbulk} + E_{bind}/2}{k_B T}\right)$, $w_4 = \nu_{bulk} \exp\left(-\frac{E_{mbulk} - E_{bind}/2}{k_B T}\right)$, where ν_{bulk} and E_{mbulk} are attempt frequency and migration energy barrier for self-diffusion in the group-V sublattice. The binding energy E_{bind} for the complex of phosphorous vacancy with the arsenic substitution atom

As_PV_P was calculated as: $E_{bind} = E_{form}(V_P) + E_{form}(As_P) - E_{form}(As_P V_P)$.

In the case of non-zero binding energy between the impurity atom and vacancy, the probability of presence of vacancy near the impurity atom is $\frac{N_{def}}{N_{sites}} \exp\left(\frac{E_{bind}}{k_B T}\right)$, and the diffusion coefficient is:

$$D = \frac{1}{6} r^2 Z f \nu \frac{N_{def}}{N_{sites}} \exp\left(-\frac{E_m}{k_B T}\right) \exp\left(\frac{E_{bind}}{k_B T}\right). \quad (7)$$

We have also calculated the diffusion coefficients via vacancies and via interstitial atoms using the KineCluE code [59], which implements the self-consistent mean-field theory for clusters of finite size. We used migration energy barriers and attempt frequencies calculated by DFT for calculation of the diffusion coefficients in this model.

3. Calculation results

3.1. Atomic structure and formation energies of group-V vacancies and complexes As_PV_P and P_{As}V_{As} in InP and InAs

Figure 1a shows the dependence of the formation energy of phosphorous vacancies in InP on the Fermi level calculated with the HSE functional for a 63-atom supercell. Convergence of

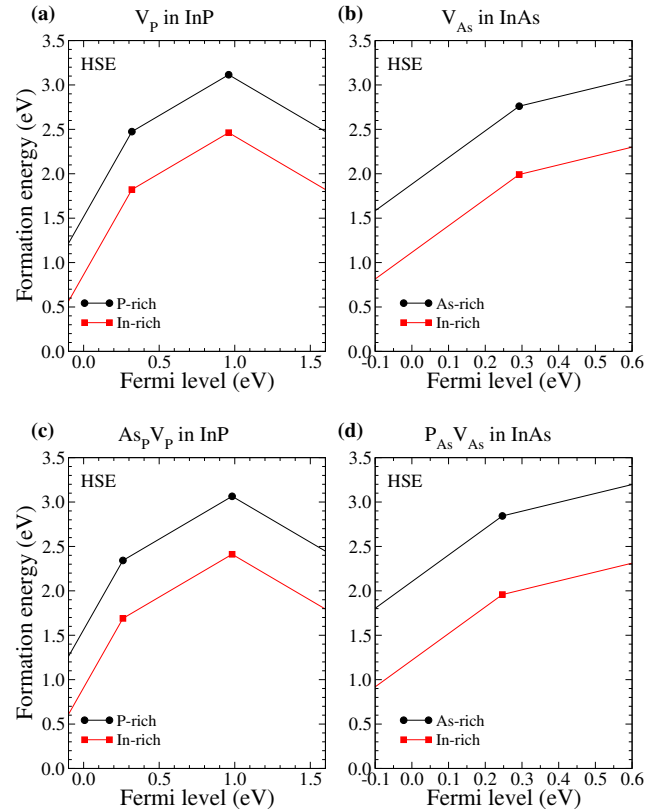


Figure 1: Dependence of the phosphorous vacancy formation energy in InP on the Fermi level for P-rich and In-rich conditions (a), dependence of the arsenic vacancy formation energy in InAs on the Fermi level for As-rich and In-rich conditions (b), and dependences of the formation energies of the As_PV_P complex in InP (c) and P_{As}V_{As} complex in InAs (d) on the Fermi level. Calculation with the hybrid HSE functional for the 63-atom supercell.

Table 1: Symmetry of V_P in InP and interatomic distances for indium atoms nearest to the vacancy in different charge states. Calculation with HSE functional for supercell size of 63 atoms. If the In-In interatomic distances are different, their number is given in parentheses for each distance. If several different configurations with close total energies are found, the difference in total energies ΔE is shown for them relative to the configuration with the minimum energy in a given charge state.

Charge	Symmetry	In-In distances, Å	ΔE , eV
+3	T_d	5.04	
+2	T_d	4.59	
+1	C_{2v}	4.71 (1), 4.18 (4), 3.39 (1)	0
+1	T_d	4.08	0.045
0	T_d	3.95	
-1	D_{2d}	3.74 (2), 3.62 (4)	

the formation energies with the supercell size was selectively checked with the PBE functional by increasing the supercell size from 64 to 216 lattice sites. The difference in the formation energies between the 216 and 64-site supercells is less than 0.10 eV for V_P in InP, 0.12 eV for V_{As} in InAs, 0.20 eV for P_i in InP and 0.16 eV for As_i in InAs (figures S1, S3a and S4a of the supplementary material to this article). For the most of the charge states of the considered defects the formation energies are sufficiently converged with the 64-site supercell, the largest difference is observed for the formation energy of the +2 charge state of the interstitials. The band gap of InP calculated with the PBE functional is 0.438 eV, this value is considerably underestimated compared to the experimental value $E_g=1.424$ eV [37]. Calculation with the hybrid HSE functional gives a value of the InP band gap $E_g=1.419$ eV which is closer to the experiment. According to calculations with the HSE functional, the charge states +3, +1 and -1 are thermodynamically stable for V_P in InP. The thermodynamic transition level (+3/+1) is 0.319 eV above the valence band edge, the thermodynamic transition level (+1/-1) is 0.960 eV above the valence band edge. The ionization energy of a singly negative vacancy is higher than the ionization energy of a neutral vacancy by 0.206 eV, which is typical for “negative-U” centers. This effect was previously observed for V_P in InP by Alatalo et al. [60]. In addition, we have observed such an effect for the thermodynamic transition (+3/+1). The values of the thermodynamic transition levels differ from the result of the work of Mishra et al. [26], in which the calculation of defect formation energies with the HSE functional was carried out for the atomic configuration relaxed in the generalized gradient approximation in a 63-atom supercell, and the thermodynamic transition level (+1/0) for V_P in InP was observed near the edge of the conduction band, and the +1 charge state was thermodynamically stable for lower Fermi levels inside the band gap. This difference is probably due to the fact that in the work of Mishra et al. [26] the energy levels of thermodynamic transitions were estimated using the Kohn-Sham levels for a neutral vacancy.

Table 1 shows the symmetry types of the phosphorus vacancy in InP for different charge states and the interatomic distances for the indium atoms nearest to the vacancy. If several different configurations with close total energies are found, interatomic

Table 2: Symmetry of V_{As} in InAs and interatomic distances for indium atoms nearest to the vacancy in different charge states. Calculation with HSE functional for supercell size of 63 atoms. If the In-In interatomic distances are different, their number is given in parentheses for each distance. If several different configurations with close total energies are found, the difference in total energies ΔE is shown for them relative to the configuration with the minimum energy in a given charge state.

Charge	Symmetry	In-In distances, Å	ΔE , eV
+3	T_d	5.22	
+2	T_d	4.67	
+1	C_{2v}	5.04 (1), 4.38 (4), 3.23 (1)	0
+1	T_d	4.20	0.035
0	T_d	3.95	
-1	T_d	3.63	0
-1	D_{2d}	3.74 (2), 3.62 (4)	0.0095

distances and the difference in total energies relative to the configuration with the minimum energy in a given charge state are also given for them. According to the calculations with the HSE functional, the P vacancy in InP in the charge states +3, +2 and 0 has T_d symmetry, in the charge state +1 it has C_{2v} symmetry with the (110) symmetry plane, and in the charge state -1 it has D_{2d} symmetry. The transition from T_d to D_{2d} symmetry with a change in the charge state of V_P in InP was observed earlier in the work of Seitsonen et al. [25], where the T_d symmetry was observed in the charge state +1 and D_{2d} symmetry was observed in charge states 0, -1, -2 in the local density approximation for V_P in InP.

For the defects considered in our study only 0 and 1/2 spin states are formed. V_P in InP has 1/2 spin in the charge states +2, 0, -2 and zero spin in the charge states +3, +1, -1, -3. The formation energies calculated with PBE functional for 64-site supercell without spin polarization for +2, 0, and -2 charge states of V_P in InP are higher by 84 meV, 17 meV and 5 meV, respectively, comparing to spin-polarized calculation. Spin-unpolarized calculation leads to 85 meV and 74 meV higher formation energies for +2 and 0 charge states of As_i in InAs, and to 119 meV and 95 meV higher formation energies for +2 and 0 charge states of P_i in InP, respectively, comparing to spin-polarized calculation.

Figure 1b shows the formation energies of V_{As} in InAs calculated with the HSE functional in dependence on the Fermi level. The charge states +3 and +1 are thermodynamically stable for V_{As} in InAs. The (+3/+1) thermodynamic transition level for V_{As} in InAs is 0.292 eV above the valence band edge. Table 2 shows the symmetry types of the arsenic vacancy in different charge states. Calculation with the HSE functional gives T_d symmetry in the charge states +3, +2, 0 and -1, and C_{2v} symmetry in the charge state +1.

To consider diffusion of As atoms in InP and P atoms in InAs by vacancy mechanism we have calculated atomic structure and formation energies of the defect complexes $As_P V_P$ in InP and $P_{As} V_{As}$ in InAs. Dependences of the formation energies of the complexes $As_P V_P$ in InP and $P_{As} V_{As}$ in InAs on the Fermi level, calculated with HSE functional for 63-atom supercell are shown in the figure 1(c,d). Thermodynamic transition levels of

Table 3: Binding energies of the complexes $\text{As}_\text{P}\text{V}_\text{P}$ in InP and $\text{P}_\text{As}\text{V}_\text{As}$ in InAs. Calculation with the PBE functional for the 63-atom supercell.

Charge	$E_{\text{bind}}(\text{As}_\text{P}\text{V}_\text{P})$, meV	$E_{\text{bind}}(\text{P}_\text{As}\text{V}_\text{As})$, meV
+3	56.9	-45.3
+1	128.7	-10.5
0	58.2	-9.6
-1	70.4	-21.3

$\text{As}_\text{P}\text{V}_\text{P}$ in InP and $\text{P}_\text{As}\text{V}_\text{As}$ in InAs are close to the levels of P vacancy in InP and As vacancy in InAs, respectively. Atomic configurations of the complexes $\text{As}_\text{P}\text{V}_\text{P}$ in InP and $\text{P}_\text{As}\text{V}_\text{As}$ in InAs have C_s symmetry with the symmetry plane (110) passing through the lattice sites with the vacancy and the substitutional atom. Binding energies of the $\text{As}_\text{P}\text{V}_\text{P}$ and $\text{P}_\text{As}\text{V}_\text{As}$ complexes are shown in the table 3.

3.2. Atomic structure and formation energies of P and As interstitial atoms in InP and InAs

Figure 2(a, b) shows formation energies of interstitial P and As atoms in InP on the Fermi level, calculated with the HSE functional. According to the calculation, the charge states +2, +1 and 0 are thermodynamically stable for P_i in InP and for As_i in InP.

Most energy favorable atomic configurations of As_i in InP for different charge states are shown in the figure 3. Split-interstitial configuration in the P atoms sublattice is energy favorable for neutral interstitial As atom (figure 3a). It has C_s symmetry and direction of the bond between P and As atoms of the split-interstitial close to the [110] direction. In the charge state +1 the most energy favorable configuration is a split-interstitial configuration in the In sublattice with C_s symmetry and direction of the bond between In and As atoms of the split-interstitial at an angle of about 20° to the [001] direction (figure 3b). In the charge state +2 the most energy favorable configuration has C_{3v} symmetry (figure 3c). In this configuration the interstitial As atom is shifted in the [111] direction from the tetrahedral interstitial site in the P atoms sublattice.

For P_i in InP the energy favorable configurations are similar to the shown in the figure 3 configurations of As_i in InP. In the neutral charge state the split-interstitial consist of two P atoms and has C_s symmetry with small deviation from C_{2v} symmetry and the direction of the bond between two P atoms close to the [110] direction. For As_i in InAs in the neutral charge state the split-interstitial consist of two As atoms and has C_{2v} symmetry and the [110] direction of the bond between two As atoms. This configuration is similar to the 110a split-interstitial As_i in GaAs in the notation of the work of Schultz et al. [61]. The split-interstitial configuration of P_i in InP in the +1 charge state is similar to the p-001g configuration of As_i in GaAs in the notation of the work of Schultz et al. [61].

Figure 2(c, d) shows the dependences of the formation energies of interstitial As and interstitial P atoms in InAs on the Fermi level, calculated with the HSE functional. According to

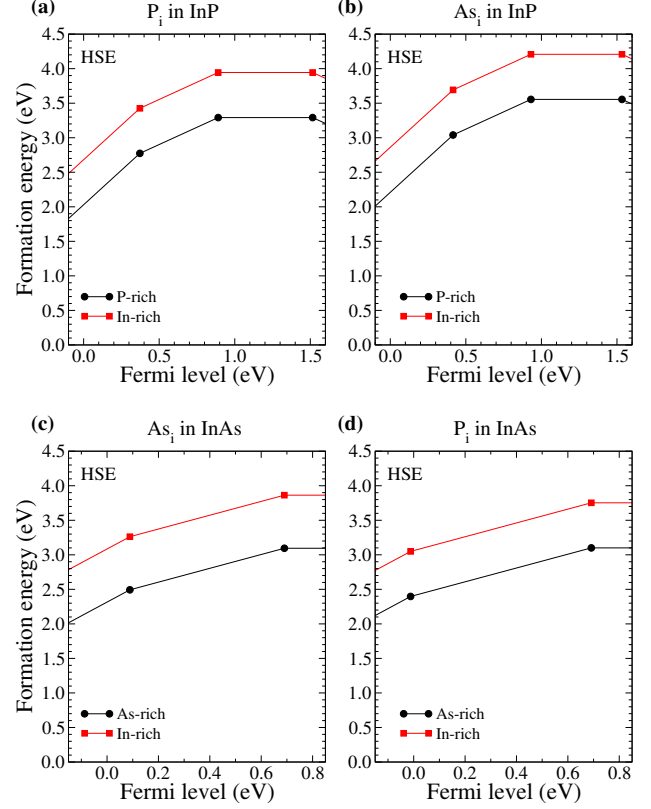


Figure 2: Dependence of the formation energy of interstitial phosphorous (a) and arsenic (b) atoms in InP on the Fermi level for P-rich and In-rich conditions, and dependence of the formation energy of interstitial As atoms (c) and interstitial P atoms (d) in InAs on the Fermi level for As-rich and In-rich conditions. Calculation with the HSE functional for the 65-atom supercell.

the calculation, the charge states +2 and +1 are thermodynamically stable for As_i in InAs at the Fermi levels inside the band gap, and the charge state +1 is thermodynamically stable for P_i in InAs at the Fermi levels inside the band gap. As_i and P_i in InAs in the charge states 0, +1, and +2 have the most energy favorable configurations similar to P_i and As_i in InP with the same symmetry types excluding the mentioned above slight difference for the neutral As_i in InAs (C_{2v} symmetry) and P_i in InP (C_s symmetry).

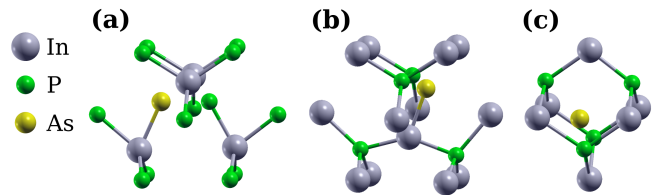


Figure 3: Energy favorable atomic configurations of the interstitial As in InP for neutral charge state (a), +1 charge state (b) and +2 charge state (c).

Table 4: Migration barriers and attempt frequencies for As atoms diffusion in InP and self-diffusion of P atoms in InP by vacancy mechanism, and pre-exponential factors for the diffusion coefficient of P vacancies in InP.

As in InP			P in InP		
Vacancy charge	E_m , eV	ν , THz	E_m , eV	ν , THz	D_0 for vacancies, cm^2/s
+3	1.453	2.53	1.734	4.62	$1.64 \cdot 10^{-2}$
+1	1.887	2.77	1.962	5.44	$1.93 \cdot 10^{-2}$
0	1.807	3.24	2.005	5.30	$1.88 \cdot 10^{-2}$
-1	1.801	3.22	1.766	6.75	$2.40 \cdot 10^{-2}$

3.3. Migration barriers for diffusion of As and P atoms in InP by vacancy mechanism

Figure 4 shows calculated energy profiles for the process of a P atom migration to the phosphorous vacancy site and a substitutional As atom migration to the phosphorous vacancy site in InP for different charge states of the vacancy. When a P atom moves to the P vacancy site in InP, the symmetry relative to the (1-10) plane, in which the initial and final lattice sites are located, is generally preserved. For the P vacancy in InP in the charge state -1 the path with a slight deviation from this plane has approximately the same energy barrier. Reflection relative to the (110) plane, which is perpendicular to the (1-10) plane, transforms the initial lattice site into the final one. The (110) plane in some cases is a plane of symmetry for the migration trajectory. For a P vacancy in InP in the charge states +1 and -1 this symmetry is broken. This asymmetry was previously observed for GaAs [18, 22, 62]. Table 4 shows the calculated migration energy barriers and the attempt frequencies for As atoms diffusion in InP and self-diffusion of P atoms in InP by vacancy mechanism, and the pre-exponential factors for diffusion coefficient of phosphorous vacancies in InP.

3.4. Migration barriers for diffusion of As and P atoms in InAs by vacancy mechanism

Figure 5 shows calculated energy profiles for the process of As and P atoms migration to the arsenic vacancy site in InAs for different charge states of the vacancy. An asymmetric diffusion trajectory is observed for an arsenic vacancy in InAs in the charge states +1 and -1, similarly to the case of a P vacancy in InP. Table 5 shows the calculation results of the migration energy barriers and attempt frequencies for the diffusion of As and P atoms in InAs by vacancy mechanism. The migration barrier for a neutral As vacancy in InAs calculated in the generalized gradient approximation is $E_m=1.79$ eV. This result is lower by 0.21 eV than the calculation in the local density approximation in the work of Reveil et al. [30] $E_m=2.0$ eV.

3.5. Migration barriers for diffusion of interstitial P and As atoms in InP.

We have considered different types of atoms transitions for diffusion via interstitial atoms. The energy barrier for rotation

Table 5: Migration barriers and attempt frequencies for P atoms diffusion in InAs and self-diffusion of As atoms in InAs by vacancy mechanism, and pre-exponential factors for the diffusion coefficient of As vacancies in InAs.

P in InAs			As in InAs		
Vacancy charge	E_m , eV	ν , THz	E_m , eV	ν , THz	D_0 for vacancies, cm^2/s
+3	1.787	4.74	1.506	2.72	$1.04 \cdot 10^{-2}$
+1	1.935	4.82	1.683	2.97	$1.13 \cdot 10^{-2}$
0	2.019	5.12	1.787	3.29	$1.25 \cdot 10^{-2}$
-1	1.738	6.58	1.625	3.32	$1.27 \cdot 10^{-2}$

of the axis of a neutral split-interstitial As_i in InP by an angle of 60° from the [110] direction to the [01-1] direction is 0.231 eV (figure 6a). The second type of rotation by an angle of 60° from the [110] direction to the [01-1] direction is shown in the figure 6b. The energy barrier for this transition is 0.249 eV. Movement of the As atom with formation of a split-interstitial near the neighbor site in the [110] direction in the P atoms sublattice and transition of the P atom from the split-interstitial site to the lattice site occurs with an energy barrier of 0.390 eV (figure 6c). In this case the C_s symmetry, that the initial and final states have, is broken for the intermediate states. The As atom leaves the symmetry plane and shifts to one of the two sides. The transition of an As atom from the split-interstitial to a P sublattice site with the formation of a split-interstitial consisting of two P atoms occurs with an energy barrier of 0.352 eV (figure 6d), while the energy of the final configuration As_iP_i is lower by 0.124 eV than the initial As_i energy, so the reverse transition has an energy barrier of 0.476 eV. This transition also occurs with C_s symmetry breaking. For each site in the P atoms sublattice, there are 12 directions of transition to the nearest sites of the P sublattice. The most energy favorable transition paths for the neutral As_i in directions non-parallel to the axis of the split-interstitial are divided into several stages: a rotation or several rotations of the axis of the split-interstitial by an angle of 60° and transition along the axis of the split-interstitial.

For the atomic configuration of As_i in charge state +1 shown in figure 3b, there are 12 symmetry equivalent configurations for one site: 6 possible arrangements of the plane in which the bonds of the In atom with the As atom and the two nearest P atoms are located, for each of which two directions of the In atom bond with the As atom are possible. The transition of the As atom with a change in the direction of the In-As bond (figure 6e) occurs with an energy barrier of 0.340 eV. In this case, the transition occurs in two stages with the movement of the As atom out of the plane in which the bonds of the In atom with the two nearest P atoms are located, and the formation of an As-P split-interstitial in the intermediate metastable state. The energy barrier for leaving the split-interstitial metastable state is 0.028 eV.

The transition of the As atom in the direction perpendicular to the plane of the bonds of the In atom with the As atom and

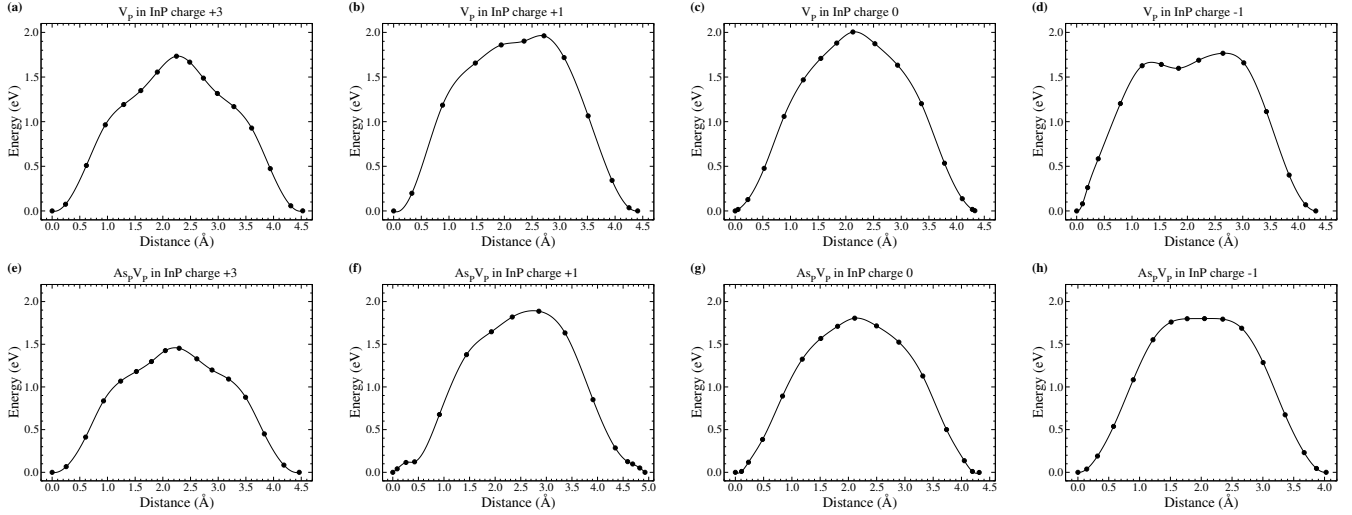


Figure 4: Energy profiles for the process of a P atom migration to the phosphorous vacancy site (a, b, c, d) and a substitutional As atom migration to the phosphorous vacancy site (e, f, g, h) in InP for different charge states of the vacancy.

the two nearest P atoms also occurs through the intermediate metastable split-interstitial state (figure 6f). In the final state of this transition, the As atom moves to the P site and an interstitial P is formed in the configuration of the In-P split-interstitial, which is close to the shown in the figure 3b configuration of the In-As split-interstitial. The energy of this state is lower by 0.145 eV than the energy of the initial configuration. The energy barriers are 0.340 eV for the transition from the initial state to the metastable state with the As-P split-interstitial configuration, and 0.115 eV for the transition from the metastable to the final state. The energy barriers for transitions in the reverse direction are 0.572 eV and 0.028 eV, respectively.

In the configuration of the In-As split-interstitial in InP in charge state +1 (figure 3b), there are 2 out of 12 nearest sites in the In sublattice for which the distance between the In and As atoms is the shortest. The transition in the direction of one of these sites with the formation in it of an In-As split-interstitial of the same configuration, but with a different direction of the In-As bond, occurs with an energy barrier of 0.781 eV (figure 6g). Two such transitions lead to the transition of the As atom to a neighbor In atom in the plane which contains the bonds of the In atom with the As atom and the two P atoms. If we assume that an As atom makes only this type of jumps, we get that it will move inside the tetrahedron formed by In atoms of the In sublattice. For the macroscopic movement of an As atom along interstitial positions, a combination of this type of transition with the transition of changing the direction of the In-As bond is necessary (figure 6e). Transitions perpendicular to the plane, in which the bonds of the In atom with the two nearest P atoms are located, through the intermediate metastable split-interstitial state (figure 6f) have a lower barrier energy and implement the indirect interstitial (interstitialcy) mechanism. Rotation of the plane, in which the bonds of the In atom with the As atom and one of the two P atoms are located, by an angle of 60° for As_i in InP in the +1 charge state occurs

with an energy barrier of 0.487 eV (figure 6h).

In the +2 charge state of the interstitial As atom in InP, the most energy favorable configuration of atoms has C_{3v} point symmetry with the As atom located inside the tetrahedron formed by P atoms and shifted to one of the faces of the tetrahedron (figure 3c). Accordingly, there are 4 equivalent positions of the interstitial As atom inside each tetrahedron. The transition between such equivalent configurations occurs with an energy barrier of 0.105 eV (figure 7). The energy profile shown in the figure 7 corresponds to the movement of an interstitial As atom in InP in the +2 charge state by one translation vector of a primitive cell. This profile contains a transition of an As atom to the nearest C_{3v} position in the nearest empty tetrahedron formed by P atoms with an energy barrier of 0.497 eV, and a transition between two equivalent C_{3v} positions inside one tetrahedron with an energy barrier of 0.105 eV. For the first transition, two local energy minima are also observed. Figure 6i shows the transition of the interstitial As atom to a substituting position in the P sublattice with the displacement of the P atom into the interstitial position. This transition has an energy barrier of 0.567 eV, and the reverse transition has an energy barrier of 0.622 eV.

Tables 6 and 7 show the calculation results of migration energy barriers and attempt frequencies for diffusion of interstitial As and P atoms in InP.

3.6. Migration barriers for diffusion of interstitial P and As atoms in InAs

Tables 8 and 9 show the calculation results of the migration energy barriers and attempt frequencies for diffusion of interstitial As and P atoms in InAs. Energy profiles for the processes of migration of interstitial As and P atoms in InAs, as well as interstitial P atoms in InP are given in the supplementary material. The migration barrier for the movement of a neutral split-interstitial $(\text{As-As})_i$ in InAs to a neighbor position in the

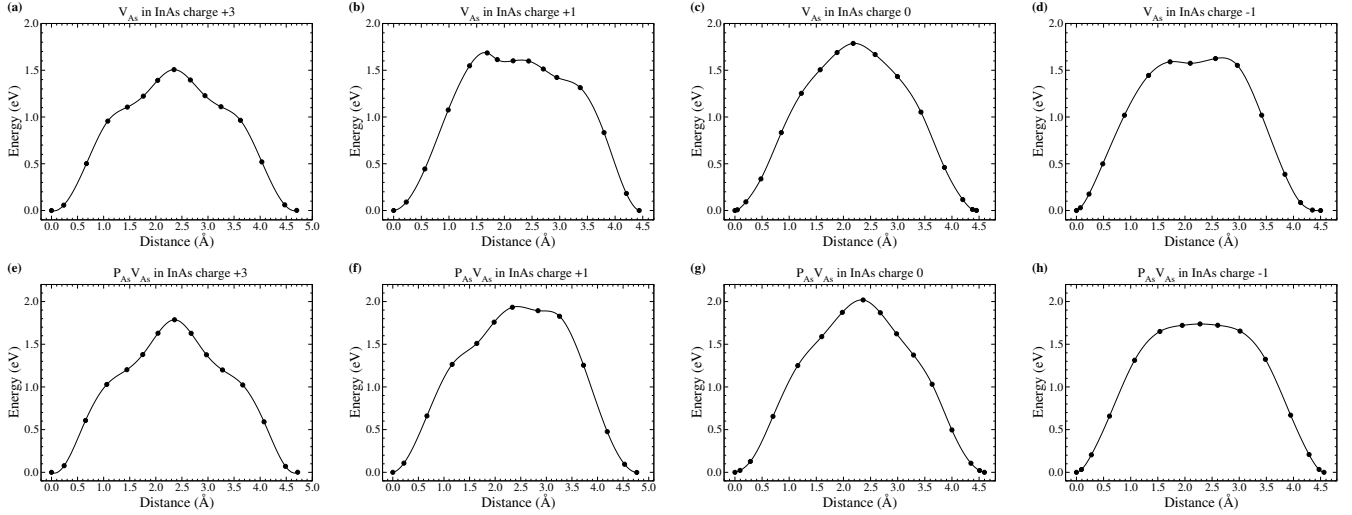


Figure 5: Energy profiles for the process of an As atom migration to the arsenic vacancy site (a, b, c, d) and a substitutional P atom migration to the arsenic vacancy site (e, f, g, h) in InAs for different charge states of the vacancy.

Table 6: Migration barriers and attempt frequencies for the diffusion of interstitial As atoms in InP.

As _i charge	Jump type	E_m , eV	ν , THz
+2	between tetrahedra	0.497	2.43
+2	between equivalent C_{3v} positions	0.105	2.43
+2	$As_i \rightarrow As_P + P_i$	0.567	3.36
+2	$As_P + P_i \rightarrow As_i$	0.622	4.13
+1	$(In-As)_i \rightarrow (In-As)_i$	0.781	1.78
+1	rotation of $(In-As)_i$	0.487	2.12
+1	$(In-As)_i \rightarrow (As-P)_i$	0.340	1.70
+1	$As_P + (In-P)_i \rightarrow (As-P)_i$	0.572	1.76
+1	$(As-P)_i \rightarrow As_P + (In-P)_i$	0.115	1.69
+1	$(As-P)_i \rightarrow (In-As)_i$	0.028	1.69
0	60° rotation of $(As-P)_i$	0.231	3.03
0	60° rotation of $(As-P)_i$, type 2	0.249	1.46
0	$(As-P)_i \rightarrow (As-P)_i$	0.390	1.69
0	$(As-P)_i \rightarrow As_P + (P-P)_i$	0.352	1.34
0	$As_P + (P-P)_i \rightarrow (As-P)_i$	0.476	1.17

Table 7: Migration barriers and attempt frequencies for the diffusion of interstitial P atoms in InP.

P _i charge	Jump type	E_m , eV	ν , THz
+2	between tetrahedra	0.447	3.89
+2	between equivalent C_{3v} positions	0.111	3.89
+2	$P_i + P_P \rightarrow P_P + P_i$	0.483	4.91
+1	$(In-P)_i \rightarrow (In-P)_i$	0.775	2.04
+1	rotation of $(In-P)_i$	0.622	2.41
+1	$(In-P)_i \rightarrow (P-P)_i$	0.425	1.65
+1	$(P-P)_i \rightarrow (In-P)_i$	0.035	1.65
0	$(P-P)_i \rightarrow (P-P)_i$	0.396	1.61
0	60° rotation of $(P-P)_i$	0.133	2.64

Table 8: Migration barriers and attempt frequencies for the diffusion of interstitial As atoms in InAs.

As _i charge	Jump type	E_m , eV	ν , THz
+2	between tetrahedra	0.358	2.13
+2	between equivalent C_{3v} positions	0.048	2.13
+2	$As_i + As_{As} \rightarrow As_{As} + As_i$	0.395	2.72
+1	$(In-As)_i \rightarrow (In-As)_i$	0.567	1.64
+1	rotation of $(In-As)_i$	0.434	1.89
+1	$(In-As)_i \rightarrow (As-As)_i$	0.307	1.40
+1	$(As-As)_i \rightarrow (In-As)_i$	0.098	1.52
0	$(As-As)_i \rightarrow (As-As)_i$	0.327	1.32
0	60° rotation of $(As-As)_i$	0.284	1.90

Table 9: Migration barriers and attempt frequencies for the diffusion of interstitial P atoms in InAs.

P _i charge	Jump type	E_m , eV	ν , THz
+2	between tetrahedra	0.360	3.27
+2	between equivalent C_{3v} positions	0.095	3.27
+2	$P_i \rightarrow P_{As} + As_i$	0.454	3.27
+2	$P_{As} + As_i \rightarrow P_i$	0.490	2.68
+1	$(In-P)_i \rightarrow (In-P)_i$	0.702	1.97
+1	rotation of $(In-P)_i$	0.566	2.23
+1	$(In-P)_i \rightarrow (P-As)_i$	0.396	1.56
+1	$P_{As} + (In-As)_i \rightarrow (P-As)_i$	0.256	1.49
+1	$(P-As)_i \rightarrow P_{As} + (In-As)_i$	0.024	1.41
+1	$(P-As)_i \rightarrow (In-P)_i$	0.117	1.41
0	60° rotation of $(P-As)_i$	0.189	1.55
0	60° rotation of $(P-As)_i$, type 2	0.166	2.50
0	$(P-As)_i \rightarrow (P-As)_i$	0.311	1.38
0	$(P-As)_i \rightarrow P_{As} + (As-As)_i$	0.415	1.13
0	$P_{As} + (As-As)_i \rightarrow (P-As)_i$	0.378	1.34

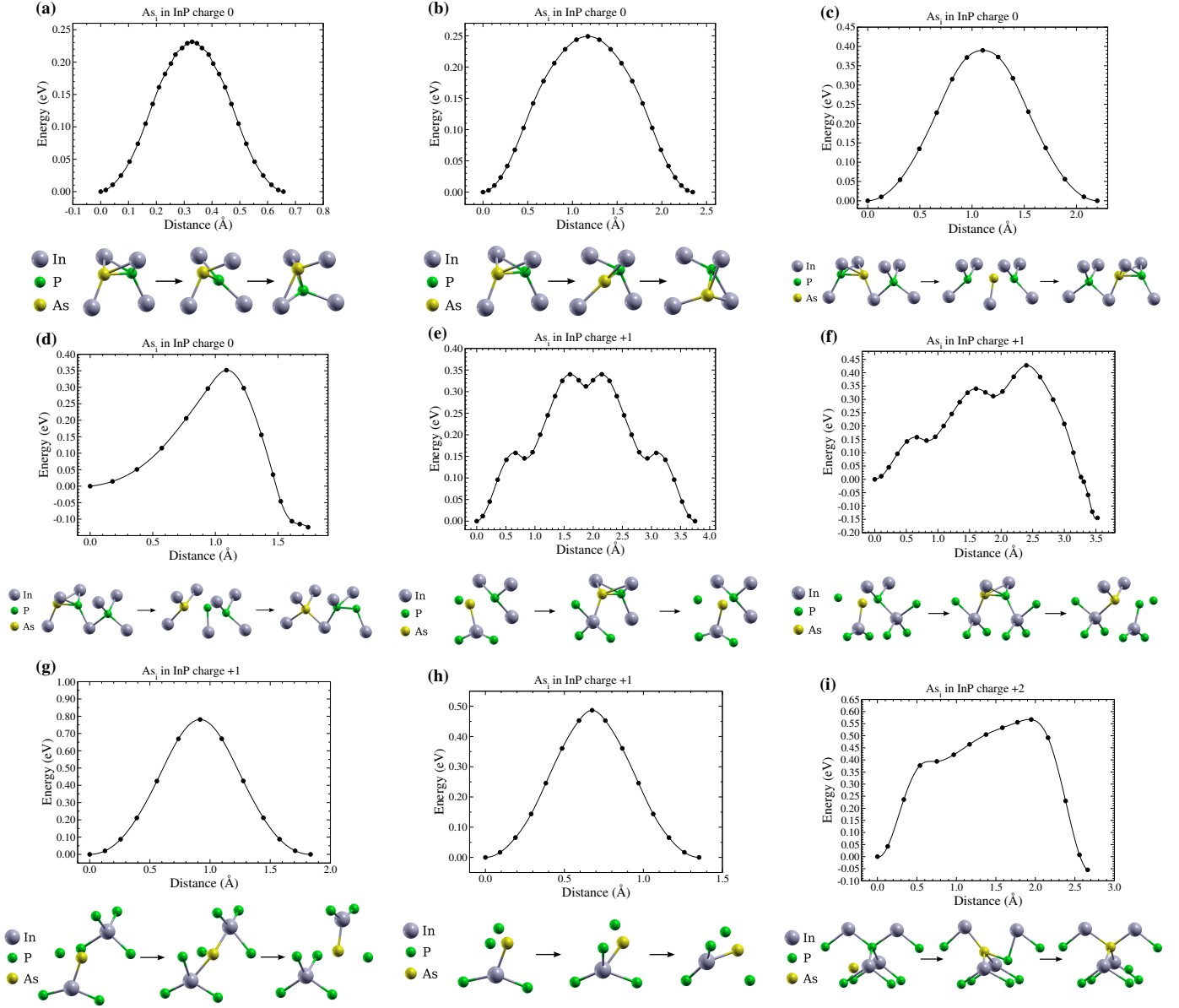


Figure 6: Energy profiles and schemes of the transitions with atomic configurations of initial state, saddle point and final state for different jump types of As_i in InP: (a) – rotation of the $(\text{As-P})_i$ split-interstitial in InP in a neutral charge state; (b) – rotation of the $(\text{As-P})_i$ split-interstitial in InP in a neutral charge state (type 2); (c) – movement of an As atom from a neutral split-interstitial with the formation of a split-interstitial near the neighboring site in the $[110]$ direction in the sublattice of P atoms in InP $(\text{As-P})_i \rightarrow (\text{As-P})_j$; (d) – transition of an As atom from a neutral split-interstitial to a P sublattice site with the formation of a split-interstitial consisting of two P atoms $(\text{As-P})_i \rightarrow \text{As}_\text{P} + (\text{P-P})_i$; (e) – transition of an interstitial As atom in InP in the charge state +1 with a change in the direction of the In-As bond through the metastable split-interstitial state $(\text{In-As})_i \rightarrow (\text{As-P})_j \rightarrow (\text{In-As})_j$, the atomic configurations of the initial state, the intermediate metastable split-interstitial state, and the final state are shown; (f) – transition of an interstitial As atom in InP in the +1 charge state in the direction perpendicular to the plane in which the bonds of the In atom with the two nearest P atoms are located through the intermediate metastable split-interstitial state, the atomic configurations of the initial state $(\text{In-As})_i \rightarrow (\text{As-P})_j \rightarrow \text{As}_\text{P} + (\text{In-P})_j$, the intermediate metastable split-interstitial state, and the final state are shown; (g) – transition of an interstitial As atom in InP in the +1 charge state from an In-As split-interstitial site to a neighboring In atom with formation of an In-As split-interstitial with different bond direction $(\text{In-As})_i \rightarrow (\text{In-As})_j$; (h) – rotation of the plane, in which the bonds of the In atom with the As atom and one of the two P atoms are located, by an angle of 60° for $(\text{In-As})_i$ in InP in the +1 charge state; (i) – transition of an interstitial As atom in InP to a substitution position in the P sublattice with the displacement of the P atom into the interstitial position for the +2 charge state $\text{As}_i \rightarrow \text{As}_\text{P} + \text{P}_i$.

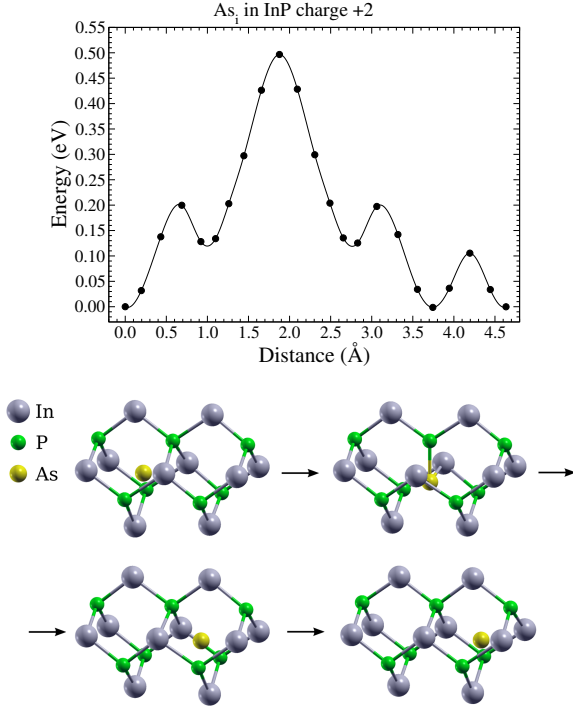


Figure 7: Migration of an interstitial As atom in InP for the +2 charge state: energy profile and scheme of the transition. The atomic configurations of the initial state, the saddle point, the nearest minimum energy C_{3v} configuration, and the final state in which the As atom is displaced by one translation vector of the primitive cell are shown.

[110] direction is $E_m=0.327$ eV, which is comparable to the result of Reveil et al. [30] for this transition $E_m=0.41$ eV. The local density approximation gives slightly higher barrier energies (0.41 eV for a neutral As_i in InAs and 2.0 eV for a neutral V_{As} in InAs [30]) than the generalized gradient approximation (0.327 eV for a neutral As_i in InAs and 1.787 eV for a neutral V_{As} in InAs). This type of transition, according to our calculations, occurs through the metastable split-interstitial state with breaking of the C_s symmetry for both P_i in InP and As_i in InAs, as well as for As_i in InP and P_i in InAs, which is consistent with the calculation of Reveil et al. [30] for As_i in InAs. A similar type of transition was also observed for neutral As_i in GaAs [21].

4. Discussion

Figure 8 shows the temperature dependences of the diffusion coefficient of P vacancies in InP and As vacancies in InAs calculated using the equation 4 with energy barriers and attempt frequencies from the tables 4 and 5. The dots in the figure 8 show the diffusion coefficients of P vacancies in InP calculated using the equation 4 with the jump rate from the experimental work of Slotte et al. [63], in which the authors used positron annihilation spectroscopy to study the diffusion of P vacancies in p-type InP. For p-InP, considering that in accordance with the figure 1a V_P are in the charge state +3, our calculation gives

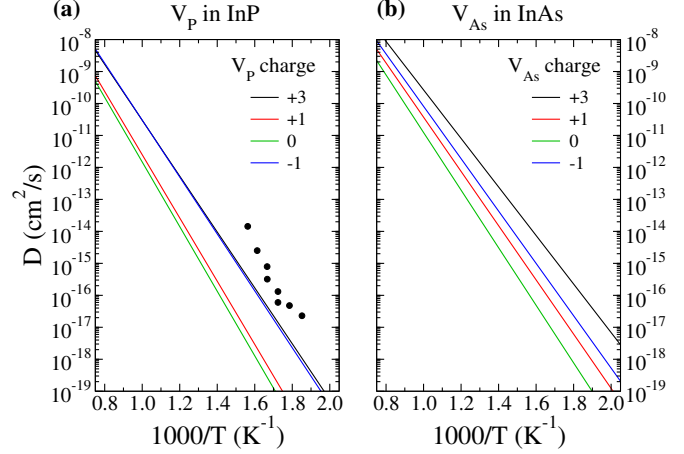


Figure 8: Calculated temperature dependences of the diffusion coefficient of vacancies of group-V elements in InP and InAs for various charge states of the vacancy (solid lines). The dots show the diffusion coefficients of P vacancies in InP calculated using the equation 4 with the jump rate from the experimental results of Slotte et al. [63] for V_P in p-type InP.

$E_m=1.734$ eV and $D_0=1.64 \cdot 10^{-2}$ cm²/s. Our results for the energy barrier for vacancy diffusion are in good agreement with the results of Slotte et al. [63] for the activation energy of diffusion $E_m=1.8 \pm 0.2$ eV. In absolute values, the experimental diffusion coefficient is 4–40 times higher than our calculations, which can be due to the presence of unaccounted migration entropy $\Delta S_m \approx 2.6k_B$.

Figure 9 shows the calculated temperature dependences of the ratio of the diffusion coefficient to the relative concentration of vacancies N_{vac}/N_{sites} for diffusion of As atoms in InP and P atoms in InAs by vacancy mechanism. The calculation was carried out according to the equation 7 with energy barriers and attempt frequencies from the tables 4 and 5, and with binding energies of the $As_P V_P$ complexes in InP and $P_{As} V_{As}$ complexes in InAs from the table 3. The correlation coefficient was calculated using the Manning model (equations 5, 6). The circles in the figure 9 show the calculation using the KineCluE code [59] with the same energy barriers, attempt frequencies and binding energies of the $As_P V_P$ and $P_{As} V_{As}$ complexes. It can be seen from the figure that both methods give very similar results for the diffusion coefficient. Table 10 shows the activation energies and pre-exponential factors obtained by fitting the calculation results shown in the figure 9 by thermally activated dependence: $D/(N_{vac}/N_{sites}) = D_0 \exp(-E_m/kT)$. We note that the D_0 factors in the table 10 do not include the factors with the formation entropy of the vacancies.

Figure 10 shows the calculated temperature dependences of the ratio of the diffusion coefficient to the relative concentration of interstitial atoms N_{def}/N_{sites} for diffusion via interstitial atoms for As and P atoms in InP and InAs. These dependencies were calculated using the KineCluE code [59] with energy barriers and attempt frequencies from the tables 6–9. In the case of asymmetric barriers, the corresponding binding energies were set from the energy profiles of migration for different configurations of the impurity atom and the defect.

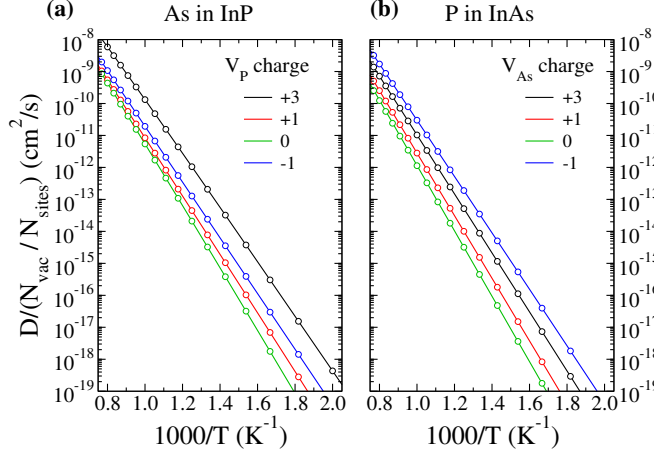


Figure 9: Calculated temperature dependences of the ratio of the diffusion coefficient to the relative concentration of vacancies for diffusion of As atoms in InP and P atoms in InAs by vacancy mechanism for various charge states of the vacancy. Solid lines show calculation with the correlation coefficient from the Manning model; circles show calculation using KineCluE code with energy barriers, attempt frequencies and binding energies from the tables 3–5.

Table 10: Migration barriers and pre-exponential factors for the ratio of the diffusion coefficient for the vacancy mechanism to the relative concentration of vacancies, taking into account the temperature dependence of the correlation coefficient and the binding energy of vacancy and impurity atom, obtained by fitting the calculation results shown in the figure 9 by thermally activated dependence: $D/(N_{vac}/N_{sites}) = D_0 \exp(-E_m/kT)$.

	As in InP		P in InAs	
Charge	E_m , eV	D_0 , cm ² /s	E_m , eV	D_0 , cm ² /s
+3	1.595	$1.59 \cdot 10^{-2}$	1.820	$1.57 \cdot 10^{-2}$
+1	1.793	$9.33 \cdot 10^{-3}$	1.932	$1.55 \cdot 10^{-2}$
0	1.862	$1.42 \cdot 10^{-2}$	2.023	$1.82 \cdot 10^{-2}$
-1	1.730	$1.01 \cdot 10^{-2}$	1.739	$1.76 \cdot 10^{-2}$

Diffusion of the neutral split-interstitials P_i in InP and As_i in InAs is determined by the activation energies of the transitions $(As-As)_i \rightarrow (As-As)_i$ and $(P-P)_i \rightarrow (P-P)_i$. Rotations have lower activation energies and they alone do not lead to macroscopic atomic motion. The diffusion coefficient of a split-interstitial as a defect without regard to which atoms form it can be calculated as

$$D_I = \frac{1}{6} r^2 f Z \nu \exp\left(-\frac{E_m}{k_B T}\right), \quad (8)$$

here $f=1$, since the jumps in different directions are independent, $Z=2$, because of at any given time only two directions are available for a jump, $r = \frac{a}{\sqrt{2}}$. The diffusion coefficient of atoms for this mechanism will be less than the diffusion coefficient of split-interstitials, since with each movement of a split interstitial one of the atoms moves to a lattice site. The diffusion coefficient of atoms in this case

$$D_{at} = \frac{1}{6} r^2 f Z \nu \frac{N_I}{N_{sites}} \exp\left(-\frac{E_m}{k_B T}\right), \quad (9)$$

where $\frac{N_I}{N_{sites}}$ is the ratio of the number of split-interstitials to the number of sites in the group-V elements sublattice. The corre-

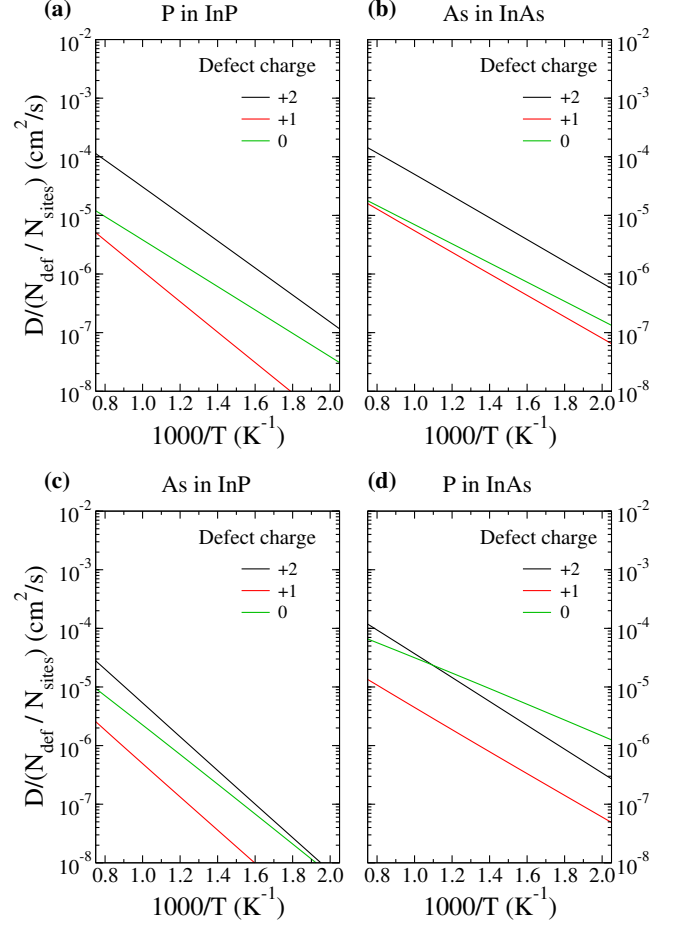


Figure 10: Calculated temperature dependences of the ratio of the diffusion coefficient via interstitial atoms to the relative concentration of interstitial atoms for P atoms in InP (a), As atoms in InAs (b), As atoms in InP (c) and P atoms in InAs (d) for various charge states of the defect. Calculation was carried out using the KineCluE code with energy barriers and attempt frequencies from the tables 6–9.

lation coefficient f in this case is less than unity. If the probability of the rotation is much greater than the jump probability, the correlation coefficient is $f = 0.4$, as follows from the modeling with the KineCluE code. For slower rotations the correlation coefficient is lower and can be approximately described by the expression

$$f \approx \frac{0.4}{1 + A \exp\left(-\frac{\Delta E}{k_B T}\right)}, \quad (10)$$

where ΔE is the difference between the barrier energies for the jump of a split-interstitial to a neighboring site and for the rotation of the split-interstitial.

For the charge states -2 and -1 of P_i and As_i in InP and InAs, the probability of a jump of an interstitial atom to a lattice site with moving of another atom from the lattice site to an interstitial position is comparable to or less than the probability of a jump from an interstitial to an interstitial position. In this case, the probability of movement only through interstitial positions decreases as the exponential function $\left(\frac{w_I}{w_I + w_S}\right)^n$ of the number of jumps n , where w_I is the rate of jumps between

interstitial positions and w_s is the rate of jumps from the interstitial to the substitutional position. At a low concentration of interstitial atoms, the time during which an impurity atom is in a substitution position significantly exceeds the time during which it is in an interstitial position, and the rate of jumps from a substitution to an interstitial position via indirect interstitial mechanism is proportional to the concentration of interstitial atoms. Thus, for all charge states of P_i and As_i in InP and InAs, the diffusion process occurs via indirect interstitial mechanism and the diffusion coefficient is proportional to the concentration of interstitial atoms.

Table 11 shows the activation energies obtained by fitting the calculation results shown in the figure 10 by thermally activated dependence: $D/(N_{def}/N_{sites}) = D_0 \exp(-E_m/kT)$. Figure 11 shows the dependence of the sum of the defect formation energy and the migration energy barrier, obtained by fitting the calculation results by a dependence of the form $D_0 \exp(-E_m/kT)$ with one activation energy (figures 8–10, tables 4, 5, 10, 11), for the diffusion of P and As atoms by vacancy and indirect interstitial mechanisms. For the vacancy diffusion mechanism, the migration energy barriers are higher than that for the interstitialcy mechanism, however, higher formation energies of the interstitial atoms lead to the fact that the total activation energies of diffusion are comparable for the vacancy and the interstitialcy mechanisms. The general trend is that for P-rich conditions in InP and As-rich conditions in InAs, the interstitial diffusion mechanism has lower activation energy, and for In-rich conditions, the vacancy diffusion mechanism has lower activation energy. However, for P atoms diffusion in n-type InAs, the diffusion activation energy for the interstitialcy mechanism is lower than that for the vacancy mechanism even under In-rich conditions.

In the work of Sallese et al. [64], the diffusion of a thin layer of InAs in InP was studied by photoluminescence measurements, the activation energy of $E_a = 3.8 \pm 0.2$ eV had been obtained, the diffusion coefficient at 830°C was $7 \cdot 10^{-17}$ cm²/s, which corresponds to $D_0 = 16.1$ cm²/s. Sallese et al. [64] performed annealing without additional phosphorus supply, so we assume that the conditions were In-rich and the dominant defects were phosphorus vacancies. Taking into account the residual electron concentration in the InP layers of the order of 10^{15} cm⁻³ [65], we will assume that the Fermi level is in the upper half of the band gap and take $E_{form} = 2.0$ eV for estimation. According to our calculations, taking into account the dependence of the correlation factor on temperature, the energy of the diffusion barrier for As diffusion in InP by the vacancy mechanism is 1.730 eV for the -1 charge state of the vacancy. In this case, the pre-exponential coefficient for the diffusion coefficient without taking into account the entropy of defect formation and migration entropy is $1.01 \cdot 10^{-2}$ cm²/s. Having estimated the activation energy for the diffusion coefficient as the sum of the formation energy and the migration energy $E_a = 3.73$ eV, we find that for agreement of the calculation with the experiment [64], it is necessary to assume $D_0 = 7.7$ cm²/s. The higher pre-exponential factor compared to the calculation is associated with the presence of additional entropy $\Delta S = 6.6 k_B$, which consists of the vacancy formation entropy and the migration en-

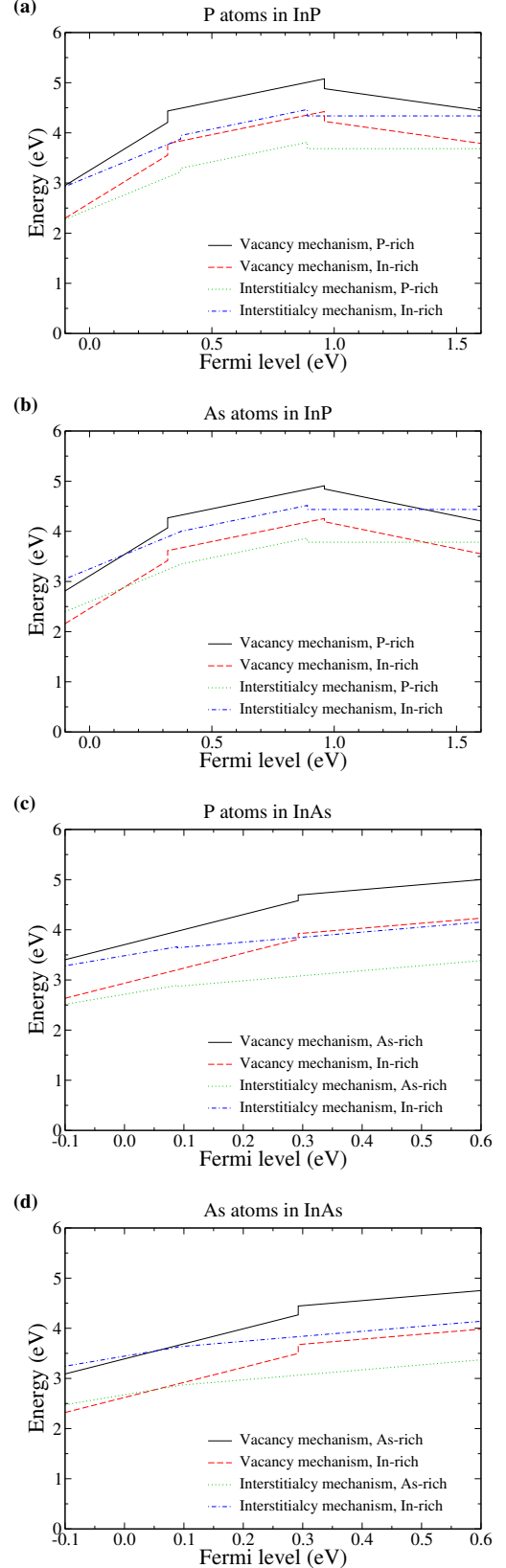


Figure 11: Dependence of the sum of the defect formation energy and the effective migration barrier energy on the Fermi level for the vacancy and indirect interstitial (interstitialcy) mechanisms of diffusion of As and P atoms in InAs and InP.

Table 11: Migration barriers and pre-exponential factors for the ratio of the diffusion coefficient for the indirect interstitial mechanism to the relative concentration of interstitial atoms, taking into account the temperature dependence of the correlation coefficient and the binding energy of the impurity atom and the defect, obtained by fitting the calculation results shown in the figure 10 by thermally activated dependence: $D/(N_{def}/N_{sites}) = D_0 \exp(-E_m/kT)$.

	As in InP		P in InP		As in InAs		P in InAs	
Charge	E_m , eV	D_0 , cm ² /s	E_m , eV	D_0 , cm ² /s	E_m , eV	D_0 , cm ² /s	E_m , eV	D_0 , cm ² /s
+2	0.568	1.6·10 ⁻²	0.449	5.6·10 ⁻³	0.359	3.3·10 ⁻³	0.399	3.8·10 ⁻³
+1	0.572	3.7·10 ⁻⁴	0.521	4.7·10 ⁻⁴	0.367	3.9·10 ⁻⁴	0.380	3.7·10 ⁻⁴
0	0.492	6.8·10 ⁻⁴	0.393	3.7·10 ⁻⁴	0.324	3.0·10 ⁻⁴	0.255	6.1·10 ⁻⁴

trophy. In this case, the entropy of vacancy formation contains a contribution from the presence of several symmetry equivalent configurations, for D_{2d} symmetry of the vacancy $N_{config}=3$. The obtained result is consistent with the results of Hurle work [66], in which the author had found $\Delta H_f=2.177$ eV and $\Delta S_f=6.09k_B$ for neutral phosphorus vacancy in InP by fitting with a thermodynamic model the experimental data on the concentration of point defects [67] obtained by precision measurements of the lattice constant and density of InP crystals.

5. Conclusions

Using density functional theory methods, the atomic structure and formation energies of group-V elements vacancies and interstitial P and As atoms in InP and InAs have been calculated and the symmetry groups of thermodynamically stable configurations of these defects have been determined. According to the calculation with the hybrid HSE functional, the phosphorus vacancy in InP has thermodynamically stable charge states +3, +1 and -1 with symmetry groups T_d , C_{2v} and D_{2d} in the corresponding charge states, the arsenic vacancy in InAs has thermodynamically stable charge states +3 and +1 with symmetry groups T_d and C_{2v} , respectively. For interstitial As and P atoms in InP and InAs in a neutral charge state, the most energy favorable configuration is the [110] split-interstitial. For As_i and P_i in InP and for As_i and P_i in InAs in the charge state +1, the most energy favorable configuration is a split-interstitial with an In atom with C_s symmetry; in the charge state +2 the configuration with C_{3v} symmetry is most energy favorable.

The main types of migration jumps for the found configurations have been determined. The most energy favorable migration paths and energy barriers of the migration transitions have been calculated. In the case of diffusion of As and P in InP and InAs via interstitial atoms the diffusion process occurs via indirect interstitial mechanism. The migration energy barriers for the vacancy diffusion mechanism are 1.60–1.86 eV for As in InP, 1.73–2.01 eV for P in InP, 1.51–1.79 eV for As in InAs, 1.74–2.02 eV for P in InAs, for different charge states. For the indirect interstitial diffusion mechanism, the migration energy barriers are lower than for the vacancy mechanism and have values of 0.49–0.57 eV for As in InP, 0.39–0.52 eV for P in InP, 0.32–0.37 eV for As in InAs, 0.26–0.40 eV for P in InAs, for different charge states.

Interstitial As and P atoms in InP and InAs have higher formation energies compared to the group-V vacancies. The to-

tal diffusion activation energies are comparable for the vacancy and the interstitial mechanisms. The vacancy diffusion mechanism gives lower activation energies for the diffusion coefficient in the case of In-rich conditions for P and As diffusion in InP, As diffusion in InAs, and P diffusion in p-type InAs. The indirect interstitial diffusion mechanism gives lower activation energies for the diffusion coefficient of P and As for P-rich conditions in InP and As-rich conditions in InAs, and also in the case of In-rich conditions for P diffusion in n-type InAs.

The temperature dependences of the diffusion coefficients of the group-V elements vacancies in InP and InAs and substitution atoms As and P in InP and InAs have been estimated for vacancy and indirect interstitial mechanisms. The results of the energy barriers calculations are consistent with experimental data [63, 64]. For agreement of the absolute values of diffusion coefficients with experiment, it is necessary to take into account the entropy of defect formation and migration entropy. The obtained results will be useful for modeling diffusion processes occurring under various experimental conditions in structures based on InP and InAs.

6. Acknowledgments

The authors greatly acknowledge support of the Ministry of Science and Higher Education of the Russian Federation within the state task of Rzhanov Institute of Semiconductor Physics SB RAS (FWGW-2022-0005). The Siberian Branch of the Russian Academy of Sciences (SB RAS) Siberian Supercomputer Center and Novosibirsk State University are gratefully acknowledged for providing computational resources.

References

- [1] J. H. Teng, J. R. Dong, S. J. Chua, M. Y. Lai, B. C. Foo, D. A. Thompson, B. J. Robinson, A. S. W. Lee, J. Hazell, I. Sproule, Controlled group V intermixing in InGaAsP quantum well structures and its application to the fabrication of two section tunable lasers, *Journal of Applied Physics* 92 (8) (2002) 4330–4335. doi:10.1063/1.1508428.
- [2] S. Blokhin, A. Babichev, L. Karachinsky, I. Novikov, A. Blokhin, M. Bobrov, A. Kuzmenkov, N. Maleev, V. Andryushkin, V. Bougrov, A. Gladyshev, D. Denisov, K. Voropaev, I. Zhumaeva, V. Ustinov, H. Li, S. Tian, S. Han, G. Sapunov, A. Egorov, D. Bimberg, 1550 nm range high-speed single-mode vertical-cavity surface-emitting lasers, *Semiconductors* 56 (8) (2022) 598. doi:10.21883/sc.2022.08.54120.9890.
- [3] B. Smiri, M. Ben Arbia, D. Ilkay, F. Saidi, Z. Othmen, B. Dkhil, A. Ismail, E. Sezai, F. Hassen, H. Maaref, Optical and structural properties of In-rich $In_xGa_{1-x}As$ epitaxial layers on (1 0 0) InP for SWIR detectors, *Materials Science and Engineering: B* 262 (2020) 114769. doi:10.1016/j.mseb.2020.114769.

- [4] D. V. Dmitriev, N. A. Valisheva, A. M. Gilinsky, I. B. Chistokhin, A. I. Toropov, K. S. Zhuravlev, InAlAs/InGaAs/InP heterostructures for microwave photodiodes grown by molecular beam epitaxy, IOP Conference Series: Materials Science and Engineering 475 (2019) 012022. doi:10.1088/1757-899x/475/1/012022.
- [5] M. Benyoucef, M. Jacob, J. P. Reithmaier, J. Kettler, P. Michler, Telecom-wavelength (1.5 μm) single-photon emission from InP-based quantum dots, Applied Physics Letters 103 (16) (2013) 162101. doi:10.1063/1.4825106.
- [6] J. Ajayan, D. Nirmal, A review of InP/InAlAs/InGaAs based transistors for high frequency applications, Superlattices and Microstructures 86 (2015) 1–19. doi:10.1016/j.spmi.2015.06.048.
- [7] M. Smit, K. Williams, J. van der Tol, Past, present, and future of InP-based photonic integration, APL Photonics 4 (5) (2019) 050901. doi:10.1063/1.5087862.
- [8] S. Bauer, V. Sichkovskiy, F. Schnabel, A. Sengül, J. P. Reithmaier, Comparison between InP-based quantum dot lasers with and without tunnel injection quantum well and the impact of rapid thermal annealing, Journal of Crystal Growth 516 (2019) 34–39. doi:10.1016/j.jcrysgro.2019.03.022.
- [9] T. S. Shamirzaev, J. Debus, D. S. Abramkin, D. Dunker, D. R. Yakovlev, D. V. Dmitriyev, A. K. Gutakovskii, L. S. Braginsky, K. S. Zhuravlev, M. Bayer, Exciton recombination dynamics in an ensemble of (In,Al)As/AlAs quantum dots with indirect band-gap and type-I band alignment, Physical Review B 84 (15) (2011) 155318. doi:10.1103/physrevb.84.155318.
- [10] H. Bracht, Self- and foreign-atom diffusion in semiconductor isotope heterostructures. I. Continuum theoretical calculations, Physical Review B 75 (3) (2007) 035210. doi:10.1103/physrevb.75.035210.
- [11] J. Bursik, D. V. Malakhov, Y. Wang, G. C. Weatherly, G. R. Purdy, Experimental investigation and modeling of diffusion in the InP/(In,Ga)As heterostructures, Journal of Applied Physics 91 (12) (2002) 9613. doi:10.1063/1.1477264.
- [12] H. Zimmermann, U. Gösele, T. Y. Tan, Diffusion of Fe in InP via the kick-out mechanism, Applied Physics Letters 62 (1) (1993) 75–77. doi:10.1063/1.108832.
- [13] I. Martin-Bragado, R. Borges, J. P. Balbuena, M. Jaraiz, Kinetic Monte Carlo simulation for semiconductor processing: A review, Progress in Materials Science 92 (2018) 1–32. doi:10.1016/j.pmatsci.2017.09.003.
- [14] R. Chen, S. T. Dunham, Correlation factors for interstitial-mediated self-diffusion in the diamond lattice: Kinetic lattice Monte Carlo approach, Physical Review B 83 (13) (2011) 134124. doi:10.1103/physrevb.83.134124.
- [15] P. E. Blöchl, E. Smargiassi, R. Car, D. B. Laks, W. Andreoni, S. T. Pantelides, First-principles calculations of self-diffusion constants in silicon, Phys. Rev. Lett. 70 (1993) 2435–2438. doi:10.1103/PhysRevLett.70.2435.
- [16] M. Posselt, F. Gao, H. Bracht, Correlation between self-diffusion in Si and the migration mechanisms of vacancies and self-interstitials: An atomistic study, Physical Review B 78 (3) (2008) 035208. doi:10.1103/physrevb.78.035208.
- [17] M. Mantina, Y. Wang, L. Chen, Z. Liu, C. Wolverton, First principles impurity diffusion coefficients, Acta Materialia 57 (14) (2009) 4102–4108. doi:10.1016/j.actamat.2009.05.006.
- [18] F. El-Mellouhi, N. Mousseau, Charge-dependent migration pathways for the Ga vacancy in GaAs, Physical Review B 74 (20) (2006) 205207. doi:10.1103/physrevb.74.205207.
- [19] K. Levasseur-Smith, N. Mousseau, Numerical characterization of the Ga interstitial self-diffusion mechanisms in GaAs, Journal of Applied Physics 103 (11) (2008) 113502. doi:10.1063/1.2936887.
- [20] G. Zollo, F. Gala, Migration barriers of neutral As di-interstitials in GaAs, New Journal of Physics 14 (5) (2012) 053036. doi:10.1088/1367-2630/14/5/053036.
- [21] A. F. Wright, N. A. Modine, Migration processes of the As interstitial in GaAs, Journal of Applied Physics 120 (21) (2016) 215705. doi:10.1063/1.4969049.
- [22] F. El-Mellouhi, N. Mousseau, Ab initio characterization of arsenic vacancy diffusion pathways in GaAs with SIEST-A-RT, Applied Physics A 86 (3) (2006) 309–312. doi:10.1007/s00339-006-3761-3.
- [23] J. T. Schick, C. G. Morgan, Gallium interstitial contributions to diffusion in gallium arsenide, AIP Advances 1 (3) (2011) 032161. doi:10.1063/1.3644937.
- [24] M. Reveil, P. Clancy, Resolving the mystery of the concentration-dependence of amphoteric dopant diffusion in III-V semiconductors, Acta Materialia 186 (2020) 555–563. doi:10.1016/j.actamat.2019.12.016.
- [25] A. P. Seitsonen, R. Virkkunen, M. J. Puska, R. M. Nieminen, Indium and phosphorus vacancies and antisites in InP, Physical Review B 49 (8) (1994) 5253–5262. doi:10.1103/physrevb.49.5253.
- [26] R. Mishra, O. D. Restrepo, A. Kumar, W. Windl, Native point defects in binary InP semiconductors, Journal of Materials Science 47 (21) (2012) 7482–7497. doi:10.1007/s10853-012-6595-8.
- [27] H. A. Tahini, A. Chroneos, S. T. Murphy, U. Schwingenschlögl, R. W. Grimes, Vacancies and defect levels in III-V semiconductors, Journal of Applied Physics 114 (6) (2013) 063517. doi:10.1063/1.4818484.
- [28] A. Chroneos, H. A. Tahini, U. Schwingenschlögl, R. W. Grimes, Antisites in III-V semiconductors: Density functional theory calculations, Journal of Applied Physics 116 (2) (2014) 023505. doi:10.1063/1.4887135.
- [29] A. Höglund, C. W. M. Castleton, S. Mirbt, Diffusion mechanism of Zn in InP and GaP from first principles, Phys. Rev. B 77 (2008) 113201. doi:10.1103/PhysRevB.77.113201.
- [30] M. Reveil, H.-L. Huang, H.-T. Chen, J. Liu, M. O. Thompson, P. Clancy, Ab Initio Studies of the Diffusion of Intrinsic Defects and Silicon Dopants in Bulk InAs, Langmuir 33 (42) (2017) 11484–11489. doi:10.1021/acs.langmuir.7b02669.
- [31] M. Reveil, J. Wang, M. O. Thompson, P. Clancy, Preferred diffusional pathways of intrinsic defects and silicon dopants in an ordered phase of In_{0.5}Ga_{0.5}As: A first-principles study, Acta Materialia 140 (2017) 39–45. doi:10.1016/j.actamat.2017.08.019.
- [32] P. Giannozzi, S. Baroni, N. Bonini, M. Calandra, R. Car, C. Cavazzoni, D. Ceresoli, G. L. Chiarotti, M. Cococcioni, I. Dabo, A. Dal Corso, S. de Gironcoli, S. Fabris, G. Fratesi, R. Gebauer, U. Gerstmann, C. Gougousis, A. Kokalj, M. Lazzeri, L. Martin-Samos, N. Marzari, F. Mauri, R. Mazzarello, S. Paolini, A. Pasquarello, L. Paulatto, C. Sbraccia, S. Scandolo, G. Sclauzero, A. P. Seitsonen, A. Smogunov, P. Umari, R. M. Wentzcovitch, QUANTUM ESPRESSO: a modular and open-source software project for quantum simulations of materials, Journal of Physics: Condensed Matter 21 (39) (2009) 395502. doi:10.1088/0953-8984/21/39/395502.
- [33] P. Giannozzi, O. Andreussi, T. Brumme, O. Bunau, M. B. Nardelli, M. Calandra, R. Car, C. Cavazzoni, D. Ceresoli, M. Cococcioni, N. Colonna, I. Carnimeo, A. Dal Corso, S. de Gironcoli, P. Delugas, R. A. DiStasio, A. Ferretti, A. Floris, G. Fratesi, G. Fugallo, R. Gebauer, U. Gerstmann, F. Giustino, T. Gorni, J. Jia, M. Kawamura, H.-Y. Ko, A. Kokalj, E. Küçükbenli, M. Lazzeri, M. Marsili, N. Marzari, F. Mauri, N. L. Nguyen, H.-V. Nguyen, A. O. de-la-Roz, L. Paulatto, S. Poncè, D. Rocca, R. Sabatini, B. Santra, M. Schlipf, A. P. Seitsonen, A. Smogunov, I. Timrov, T. Thonhauser, P. Umari, N. Vast, X. Wu, S. Baroni, Advanced capabilities for materials modelling with Quantum ESPRESSO, Journal of Physics: Condensed Matter 29 (46) (2017) 465901. doi:10.1088/1361-648x/aa8f79.
- [34] J. Heyd, G. E. Scuseria, M. Ernzerhof, Hybrid functionals based on a screened Coulomb potential, The Journal of Chemical Physics 118 (18) (2003) 8207–8215. doi:10.1063/1.1564060.
- [35] J. Heyd, G. E. Scuseria, M. Ernzerhof, Erratum: “Hybrid functionals based on a screened Coulomb potential” [J. Chem. Phys. 118, 8207 (2003)], The Journal of Chemical Physics 124 (21) (2006) 219906. doi:10.1063/1.2204597.
- [36] J. P. Perdew, K. Burke, M. Ernzerhof, Generalized Gradient Approximation Made Simple, Physical Review Letters 77 (18) (1996) 3865–3868. doi:10.1103/physrevlett.77.3865.
- [37] I. Vurgaftman, J. R. Meyer, L. R. Ram-Mohan, Band parameters for III–V compound semiconductors and their alloys, Journal of Applied Physics 89 (11) (2001) 5815–5875. doi:10.1063/1.1368156.
- [38] D. R. Hamann, Optimized norm-conserving Vanderbilt pseudopotentials, Physical Review B 88 (8) (2013) 085117. doi:10.1103/physrevb.88.085117.
- [39] M. van Setten, M. Giantomassi, E. Bousquet, M. Verstraete, D. Hamann, X. Gonze, G.-M. Rignanese, The PseudoDojo: Training and grading a 85 element optimized norm-conserving pseudopotential table, Computer Physics Communications 226 (2018) 39–54. doi:10.1016/j.cpc.

- 2018.01.012.
- [40] C. Freysoldt, J. Neugebauer, C. G. Van de Walle, Fully Ab Initio Finite-Size Corrections for Charged-Defect Supercell Calculations, *Physical Review Letters* 102 (1) (2009) 016402. doi:10.1103/physrevlett.102.016402.
 - [41] C. Freysoldt, J. Neugebauer, C. G. Van de Walle, Electrostatic interactions between charged defects in supercells, *physica status solidi (b)* 248 (5) (2010) 1067–1076. doi:10.1002/pssb.201046289.
 - [42] R. Neidert, S. Binari, T. Weng, Dielectric constant of semi-insulating indium phosphide, *Electronics Letters* 18 (23) (1982) 987. doi:10.1049/el:19820675.
 - [43] M. Hass, B. Henvis, Infrared lattice reflection spectra of III–V compound semiconductors, *Journal of Physics and Chemistry of Solids* 23 (8) (1962) 1099–1104. doi:10.1016/0022-3697(62)90127-0.
 - [44] C. G. Van de Walle, J. Neugebauer, First-principles calculations for defects and impurities: Applications to III-nitrides, *Journal of Applied Physics* 95 (8) (2004) 3851–3879. doi:10.1063/1.1682673.
 - [45] C. Freysoldt, B. Grabowski, T. Hickel, J. Neugebauer, G. Kresse, A. Janotti, C. G. Van de Walle, First-principles calculations for point defects in solids, *Reviews of Modern Physics* 86 (1) (2014) 253–305. doi:10.1103/revmodphys.86.253.
 - [46] G. Henkelman, B. P. Uberuaga, H. Jónsson, A climbing image nudged elastic band method for finding saddle points and minimum energy paths, *The Journal of Chemical Physics* 113 (22) (2000) 9901–9904. doi:10.1063/1.1329672.
 - [47] V. P. Vasil'ev, J. C. Gachon, Thermodynamic properties of InP, *Inorganic Materials* 42 (11) (2006) 1171–1175. doi:10.1134/s002016850611001x.
 - [48] K. Yamaguchi, Y. Takeda, K. Kameda, K. Itagaki, Measurements of Heat of Formation of GaP, InP, GaAs, InAs, GaSb and InSb, *Materials Transactions, JIM* 35 (9) (1994) 596–602. doi:10.2320/matertrans1989.35.596.
 - [49] B. Grabowski, L. Ismer, T. Hickel, J. Neugebauer, Ab initio up to the melting point: Anharmonicity and vacancies in aluminum, *Physical Review B* 79 (13) (2009) 134106. doi:10.1103/physrevb.79.134106.
 - [50] X. Zhang, B. Grabowski, T. Hickel, J. Neugebauer, Calculating free energies of point defects from ab initio, *Computational Materials Science* 148 (2018) 249–259. doi:10.1016/j.commatsci.2018.02.042.
 - [51] O. M. Khreis, W. P. Gillin, K. P. Homewood, Interdiffusion: A probe of vacancy diffusion in III-V materials, *Physical Review B* 55 (23) (1997) 15813–15818. doi:10.1103/physrevb.55.15813.
 - [52] J. R. Manning, Correlation Factors for Impurity Diffusion—fcc Lattice, *Physical Review* 128 (5) (1962) 2169–2174. doi:10.1103/physrev.128.2169.
 - [53] N. Peterson, Self-diffusion in pure metals, *Journal of Nuclear Materials* 69-70 (1978) 3–37. doi:10.1016/0022-3115(78)90234-9.
 - [54] H. Mehrer, *Diffusion in Solids*, Springer Berlin Heidelberg, 2007. doi:10.1007/978-3-540-71488-0.
 - [55] G. H. Vineyard, Frequency factors and isotope effects in solid state rate processes, *Journal of Physics and Chemistry of Solids* 3 (1-2) (1957) 121–127. doi:10.1016/0022-3697(57)90059-8.
 - [56] I. A. Aleksandrov, T. V. Malin, K. S. Zhuravlev, S. V. Trubina, S. B. Erenburg, B. Pecz, Y. V. Lebiadok, Diffusion in GaN/AlN superlattices: DFT and EXAFS study, *Applied Surface Science* 515 (2020) 146001. doi:10.1016/j.apsusc.2020.146001.
 - [57] K. Compaan, Y. Haven, Correlation factors for diffusion in solids. Part 2.—Indirect interstitial mechanism, *Trans. Faraday Soc.* 54 (0) (1958) 1498–1508. doi:10.1039/tf9585401498.
 - [58] J. R. Manning, Correlation Factors for Impurity Diffusion. bcc, Diamond, and fcc Structures, *Physical Review* 136 (6A) (1964) A1758–A1766. doi:10.1103/physrev.136.a1758.
 - [59] T. Schuler, L. Messina, M. Nastar, KineCluE: A kinetic cluster expansion code to compute transport coefficients beyond the dilute limit, *Computational Materials Science* 172 (2020) 109191. doi:10.1016/j.commatsci.2019.109191.
 - [60] M. Alatalo, R. M. Nieminen, M. J. Puska, A. P. Seitsonen, R. Virkkunen, Phosphorus vacancy in InP: A negative-U center, *Physical Review B* 47 (11) (1993) 6381–6384. doi:10.1103/physrevb.47.6381.
 - [61] P. A. Schultz, O. A. von Lilienfeld, Simple intrinsic defects in gallium arsenide, *Modelling and Simulation in Materials Science and Engineering* 17 (8) (2009) 084007. doi:10.1088/0965-0393/17/8/084007.
 - [62] Y. A. Du, S. Sakong, P. Kratzer, As vacancies, Ga antisites, and Au impurities in zinc blende and wurtzite GaAs nanowire segments from first principles, *Physical Review B* 87 (7) (2013) 075308. doi:10.1103/physrevb.87.075308.
 - [63] J. Slotte, K. Saarinen, A. Salmi, S. Simula, R. Aavikko, P. Hautojärvi, Formation of vacancy-impurity complexes in heavily Zn-doped InP, *Physical Review B* 67 (11) (2003) 115209. doi:10.1103/physrevb.67.115209.
 - [64] J. M. Sallese, S. Taylor, H. J. Bühlmann, J. F. Carlin, A. Rudra, R. Houdré, M. Illegems, As/P interdiffusion in ultrathin InAs/InP strained quantum wells, *Applied Physics Letters* 65 (3) (1994) 341–343. doi:10.1063/1.112365.
 - [65] A. Rudra, J. Carlin, M. Proctor, M. Illegems, Luminescence and transport properties of high quality InP grown by CBE between 450 and 550 °C, *Journal of Crystal Growth* 111 (1-4) (1991) 589–593. doi:10.1016/0022-0248(91)91045-c.
 - [66] D. T. J. Hurle, A thermodynamic analysis of native point defect and dopant solubilities in zinc-blende III–V semiconductors, *Journal of Applied Physics* 107 (12) (2010) 121301. doi:10.1063/1.3386412.
 - [67] A. N. Morozov, V. T. Bublik, V. B. Osvenskii, A. V. Berkova, E. V. Mikryukova, A. Y. Nashelskii, S. V. Yakobson, A. D. Popov, Nature and concentration of proper point defects in undoped InP monocrystals, *Sov. Phys. Crystallogr.* 28 (1983) 458.

Supplementary material to “Migration barriers for diffusion of As and P atoms in InP and InAs via vacancies and interstitial atoms”

Ivan A. Aleksandrov, Konstantin S. Zhuravlev

Rzhanov Institute of Semiconductor Physics, Siberian Branch of Russian Academy of Sciences,
Novosibirsk, Russia

1. Defect formation energies in InP and InAs in the generalized gradient approximation

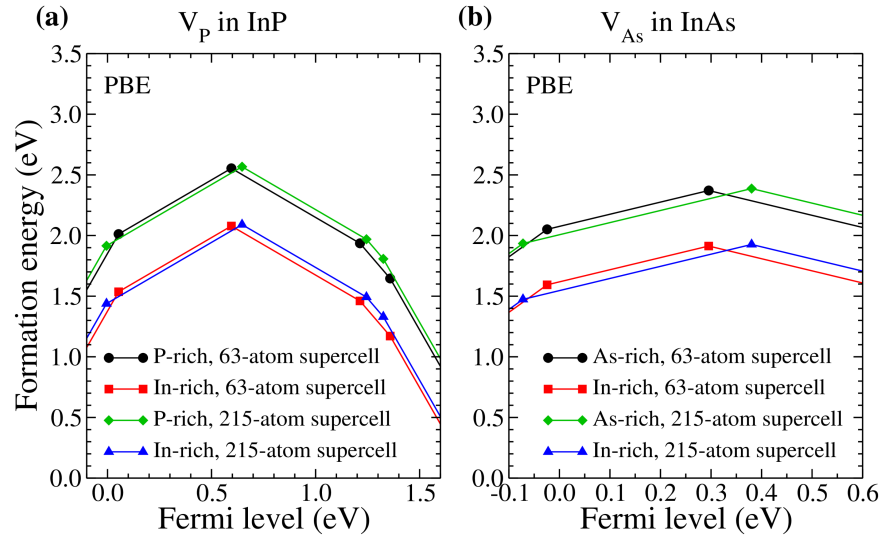


Figure S1. Dependence of the phosphorous vacancy formation energy in InP on the Fermi level for P-rich and In-rich conditions (a) and dependence of the arsenic vacancy formation energy in InAs on the Fermi level for As-rich and In-rich conditions (b). Calculation in the generalized gradient approximation with the PBE functional for the 63-atom and 215-atom supercells.

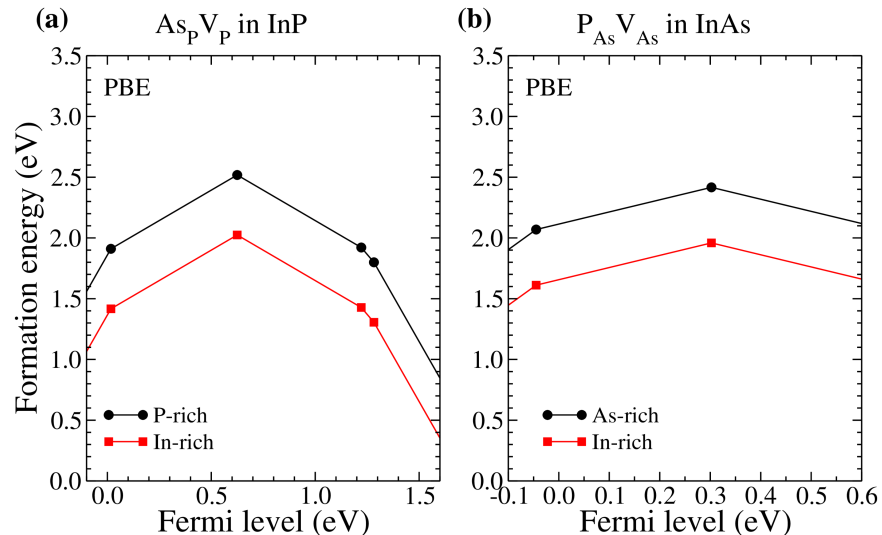


Figure S2. Dependence of the formation energies of the $As_P V_P$ complex in InP (a) and $P_{As} V_{As}$ complex in InAs (b) on the Fermi level. Calculation in the generalized gradient approximation with the PBE functional for the 63-atom supercell.

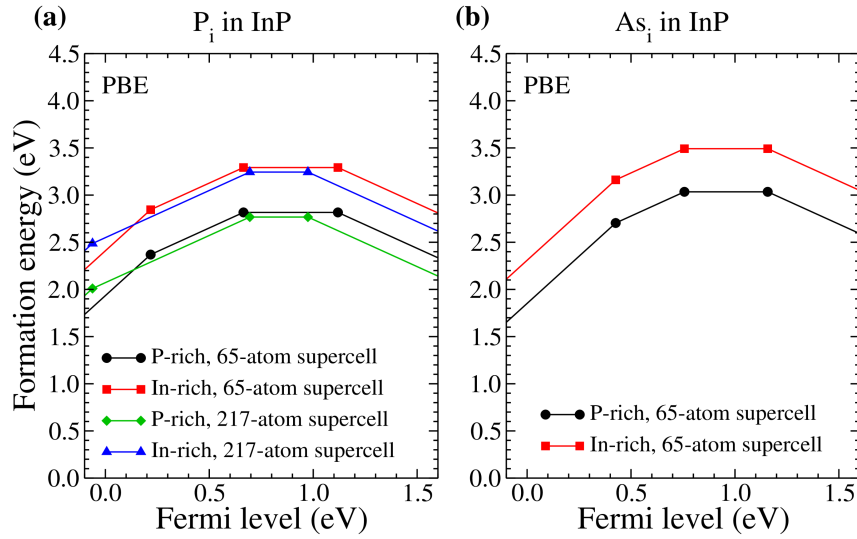


Figure S3. Dependence of the formation energy of interstitial phosphorous (a) and arsenic (b) atoms in InP on the Fermi level for P-rich and In-rich conditions. Calculation in the generalized gradient approximation with the PBE functional for the 65-atom and 217-atom supercells.

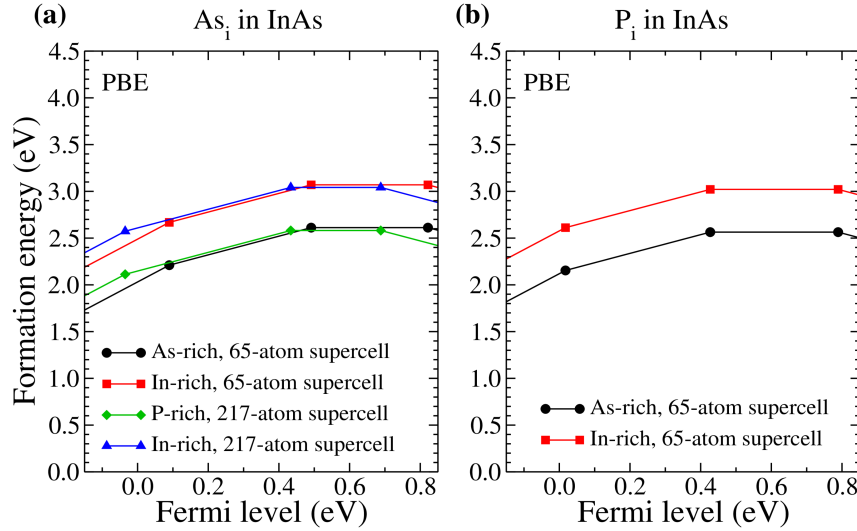


Figure S4. Dependence of the formation energy of the interstitial As atoms (a) and interstitial P atoms (b) in InAs on the Fermi level for As-rich and In-rich conditions. Calculation in the generalized gradient approximation with the PBE functional for the 65-atom and 217-atom supercells.

Table S1. Symmetry of V_P in InP and interatomic distances for indium atoms nearest to the vacancy in different charge states. Calculation with PBE functional for supercell sizes of 63 and 215 atoms. If the In-In interatomic distances are different, their number is given in parentheses for each distance. If several different configurations with close total energies are found, the difference in total energies ΔE is shown for them relative to the configuration with the minimum energy in a given charge state.

PBE, 63-atom supercell			
Charge	Symmetry	In-In distances, Å	ΔE , eV
+3	T_d	5.11	
+2	T_d	4.63	
+1	C_{2v}	4.76 (1), 4.23 (4), 3.45 (1)	0

	T_d	4.11	0.045
0	T_d	3.87	0
	C_{2v}	4.40 (1), 4.98 (4), 3.46 (1)	0.016
-1	D_{2d}	3.22 (2), 3.85 (4)	
-2	D_2	3.19 (2), 3.62 (4), 3.71 (2)	
-3	D_{2d}	3.67 (2), 3.21 (4)	
PBE, 215-atom supercell			
Charge	Symmetry	In-In distances, Å	ΔE , eV
+3	T_d	5.15	
+2	T_d	4.63	
+1	C_{2v}	4.76 (1), 4.22 (4), 3.41 (1)	0
	T_d	4.06	0.034
0	D_{2d}	3.56 (2), 3.90 (4)	0
	T_d	3.86	0.058
-1	D_{2d}	3.14 (2), 3.86 (4)	
-2	D_{2d}	3.13 (2), 3.75 (4)	
-3	D_{2d}	3.68 (2), 3.19 (4)	

Table S2. Symmetry of V_{As} in InAs and interatomic distances for indium atoms nearest to the vacancy in different charge states. Calculation with PBE functional for supercell sizes of 63 and 215 atoms. If the In-In interatomic distances are different, their number is given in parentheses for each distance. If several different configurations with close total energies are found, the difference in total energies ΔE is shown for them relative to the configuration with the minimum energy in a given charge state.

PBE, 63-atom supercell			
Charge	Symmetry	In-In distances, Å	ΔE , eV
+3	T_d	5.28	
+2	T_d	4.80	0
	C_{2v}	5.17 (1), 4.49 (4), 3.27 (1)	0.271
+1	C_{2v}	5.14 (1), 4.46 (4), 3.28 (1)	0
	T_d	4.19	0.109
0	C_{2v}	4.32 (1), 3.98 (4), 3.55 (1)	0
	T_d	3.93	0.0026
-1	T_d	3.70	
-2	D_{2d}	3.24 (2), 3.70 (4)	
-3	D_{2d}	3.70 (2), 3.24 (4)	0
	D_{2d}	3.15 (2), 3.58 (4)	0.027
PBE, 215-atom supercell			
Charge	Symmetry	In-In distances, Å	ΔE , eV
+3	T_d	5.33	
+2	C_{2v}	5.10 (1), 4.41 (4), 3.27 (1)	0
	T_d	4.77	0.124
+1	C_{2v}	5.08 (1), 4.41 (4), 3.27 (1)	0
	T_d	4.10	0.119
0	C_{2v}	4.65 (1), 4.13 (4), 3.37 (1)	0
	T_d	3.91	0.013
-1	D_{2d}	3.16 (2), 3.90 (4)	0
	T_d	3.70	0.028
-2	D_{2d}	3.14 (2), 3.83 (4)	
-3	D_{2d}	3.13 (2), 3.75 (4)	0
	D_{2d}	3.71 (2), 3.22 (4)	0.058

2. Diffusion of interstitial P atoms in InP

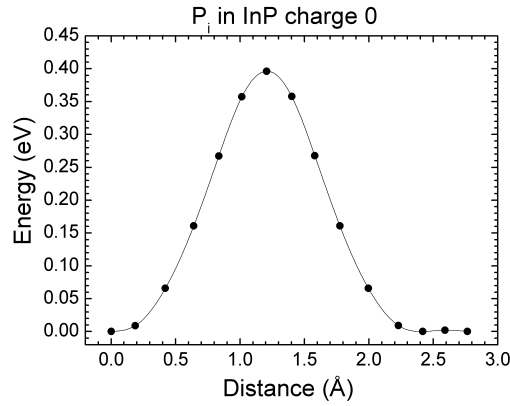


Figure S5. Energy profile for movement of a P atom from a neutral split-interstitial with the formation of a split-interstitial near the neighbor site in the [110] direction in the sublattice of P atoms in InP $(P-P)_i \rightarrow (P-P)_i$.

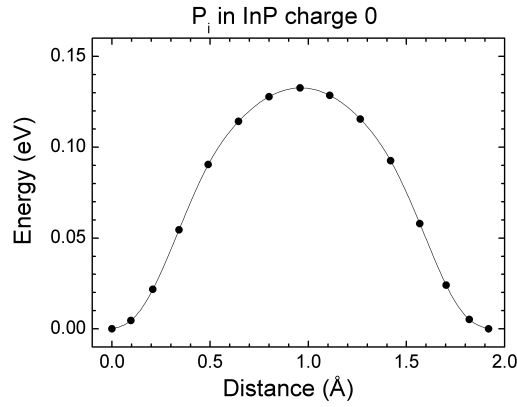


Figure S6. Energy profile for 60° rotation of the $(P-P)_i$ split-interstitial axis in InP in a neutral charge state.

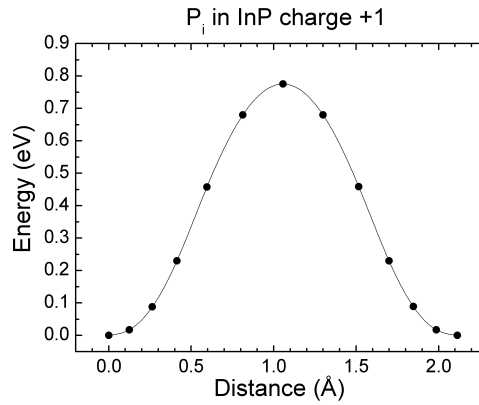


Figure S7. Energy profile for transition of an interstitial P atom in InP in the +1 charge state from an In-P split-interstitial site to a neighbor In atom with formation of an In-P split-interstitial with different bond direction $(In-P)_i \rightarrow (In-P)_i$.

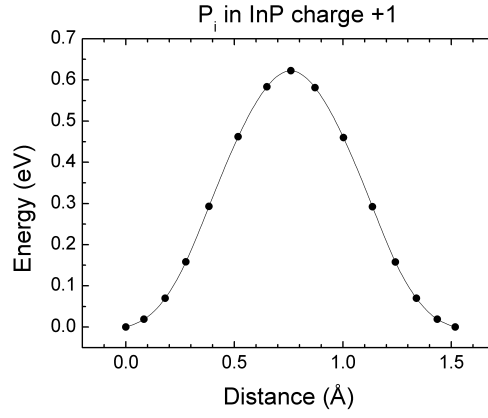


Figure S8. Energy profile for rotation of the plane, in which the bonds of the In atom with the interstitial P atom and one of the two P atoms are located, by an angle of 60° for P_i in InP in the +1 charge state.

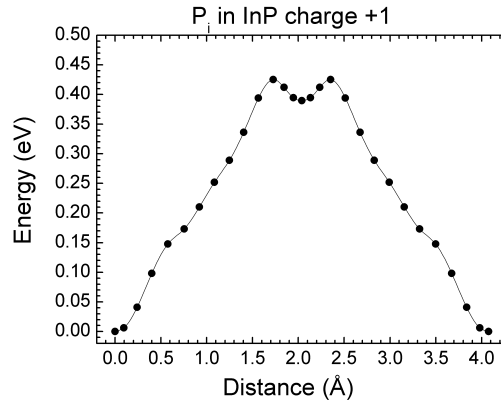


Figure S9. Energy profile for transition of an interstitial phosphorous atom in InP in the charge state +1 with a change in the direction of the In-P bond through the metastable split-interstitial state $(\text{In-P})_i \rightarrow (\text{P-P})_i \rightarrow (\text{In-P})_i$.

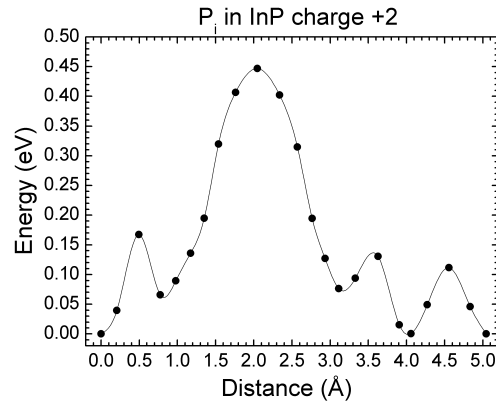


Figure S10. Energy profile for migration of an interstitial P atom in InP between the C_{3v} interstitial positions displaced by one translation vector of the primitive cell for the +2 charge state.

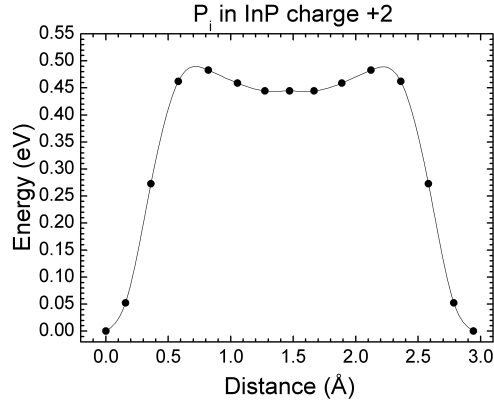


Figure S11. Energy profile for transition of an interstitial P atom in InP to a substitution position in the P sublattice with the displacement of the P atom into the interstitial position for the +2 charge state $P_i + P_P \rightarrow P_P + P_i$.

3. Diffusion of interstitial As atoms in InAs

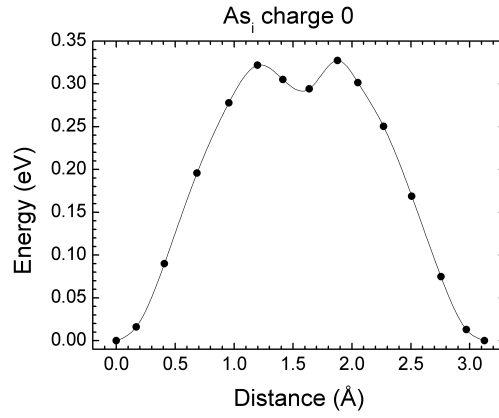


Figure S12. Energy profile for movement of a As atom from a neutral split-interstitial with the formation of a split-interstitial near the neighbor site in the [110] direction in the sublattice of As atoms in InAs $(As-As)_i \rightarrow (As-As)_i$.

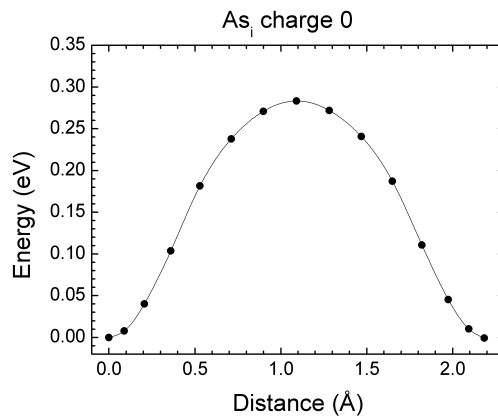


Figure S13. Energy profile for 60° rotation of the $(As-As)_i$ split-interstitial in InAs in a neutral charge state.

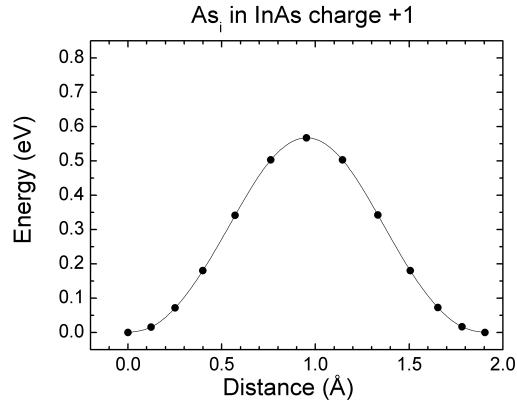


Figure S14. Energy profile for transition of an interstitial As atom in InAs in the +1 charge state from an In-As split-interstitial site to a neighbor In atom with formation of an In-As split-interstitial with different bond direction $(\text{In-As})_i \rightarrow (\text{In-As})_i$.

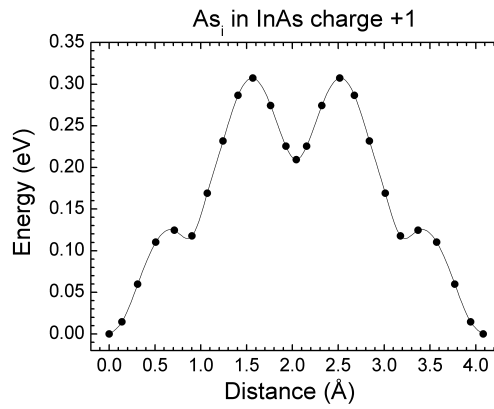


Figure S15. Energy profile for transition of an interstitial arsenic atom in InAs in the charge state +1 with a change in the direction of the In-As bond through the metastable split-interstitial state $(\text{In-As})_i \rightarrow (\text{As-As})_i \rightarrow (\text{In-As})_i$.

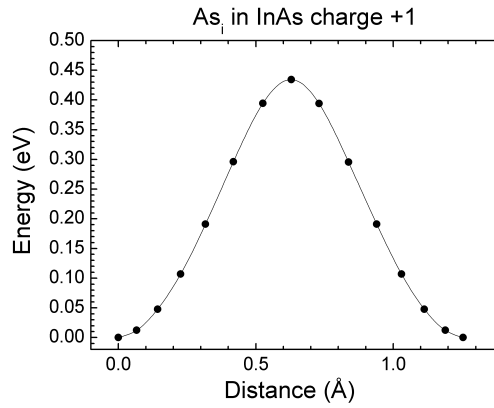


Figure S16. Energy profile for rotation of the plane, in which the bonds of the In atom with the interstitial As atom and one of the two As atoms are located, by an angle of 60° for As_i in InAs in the +1 charge state.

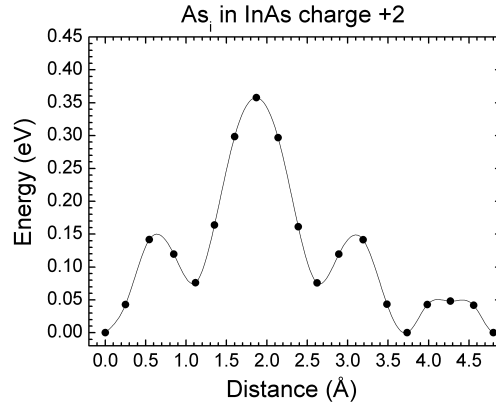


Figure S17. Energy profile for migration of an interstitial As atom in InAs between the C_{3v} interstitial positions displaced by one translation vector of the primitive cell for the +2 charge state.

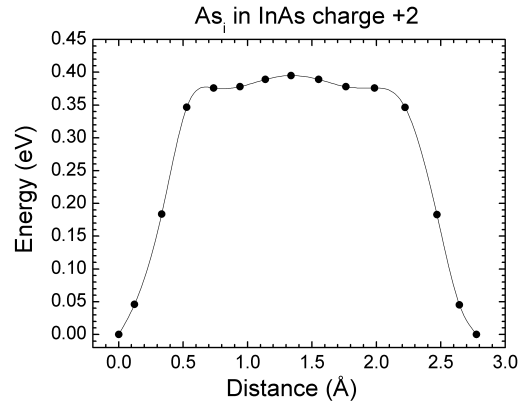


Figure S18. Energy profile for transition of an interstitial As atom in InAs to a substitution position in the As sublattice with the displacement of the As atom into the interstitial position for the +2 charge state $As_i + As_{As} \rightarrow As_{As} + As_i$.

4. Diffusion of interstitial P atoms in InAs

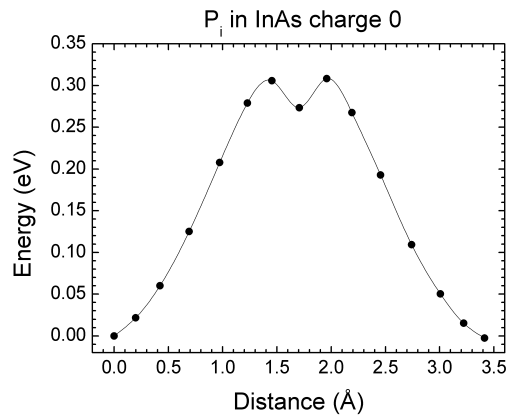


Figure S19. Energy profile for movement of a P atom from a neutral split-interstitial with the formation of a split-interstitial near the neighboring site in the [110] direction in the sublattice of As atoms in InAs $(P-As)_i \rightarrow (P-As)_i$.

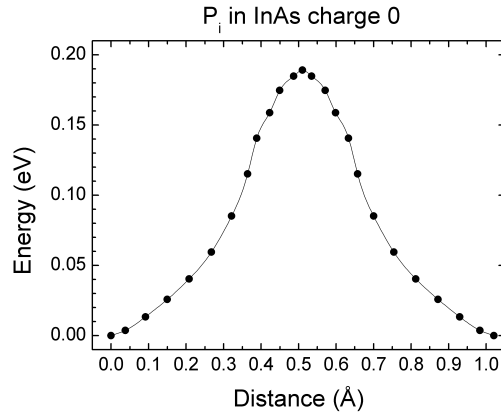


Figure S20. Energy profile for 60° rotation of the $(P-P)_i$ split-interstitial in InAs in a neutral charge state.

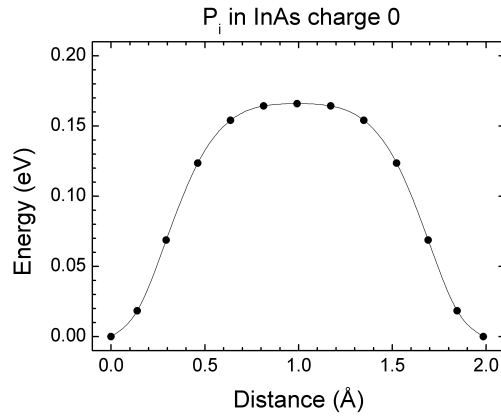


Figure S21. Energy profile for 60° rotation (type 2) of the P_i split-interstitial axis in InAs in a neutral charge state.

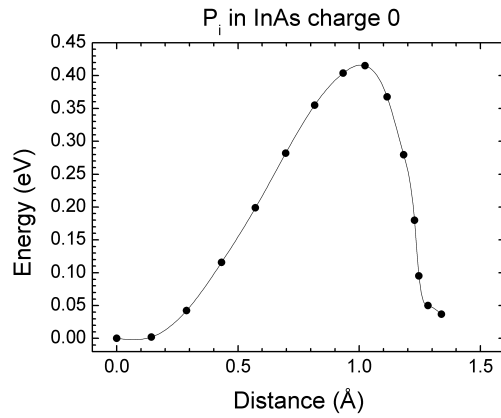


Figure S22. Transition of a P atom from a neutral split-interstitial to an As sublattice site with the formation of a split-interstitial consisting of two As atoms $(P-As)_i \rightarrow P_{As} + (As-As)_i$.

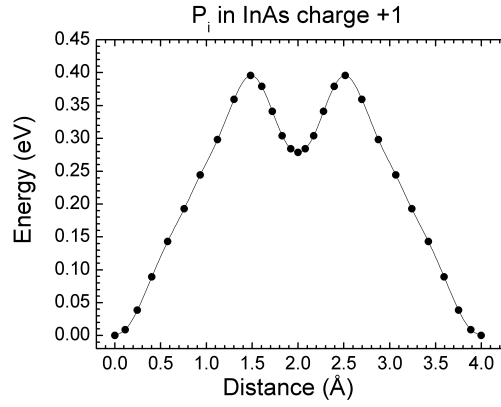


Figure S23. Energy profile for transition of an interstitial phosphorous atom in InAs in the charge state +1 with a change in the direction of the In-P bond through the metastable split-interstitial state $(\text{In-P})_i \rightarrow (\text{P-As})_i \rightarrow (\text{In-P})_i$.

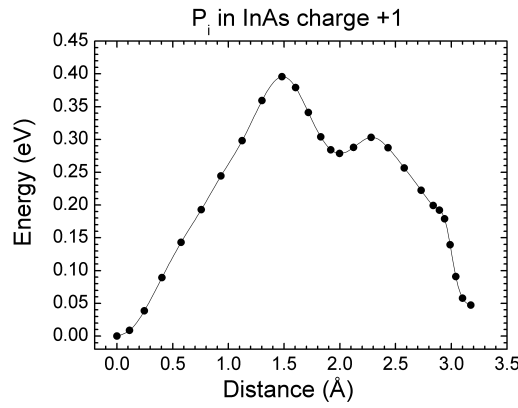


Figure S24. Energy profile for transition of an interstitial phosphorous atom in InAs in the charge state +1 in the direction perpendicular to the plane in which the bonds of the In atom with the two nearest As atoms are located through the intermediate metastable split-interstitial state $(\text{In-P})_i \rightarrow (\text{P-As})_i \rightarrow \text{P}_{\text{As}} + (\text{In-As})_i$.

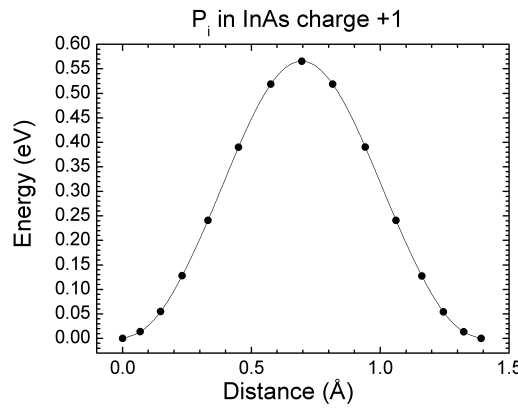


Figure S25. Energy profile for rotation of the plane in which the bonds of the In atom with the interstitial P atom and one of the two As atoms are located by an angle of 60° for P_i in InAs in the +1 charge state.

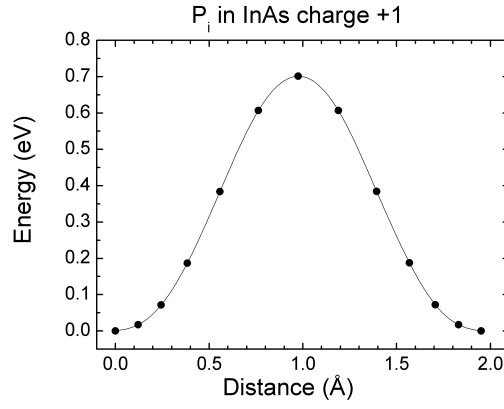


Figure S26. Energy profile for transition of an interstitial P atom in InAs in the +1 charge state from an In-P split-interstitial site to a neighbor In atom with formation of an In-P split-interstitial with different bond direction $(\text{In-P})_i \rightarrow (\text{In-P})_i$.

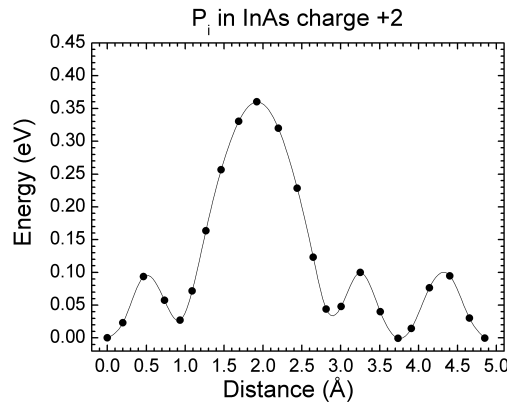


Figure S27. Energy profile for migration of an interstitial P atom in InAs between the C_{3v} interstitial positions displaced by one translation vector of the primitive cell for the +2 charge state.

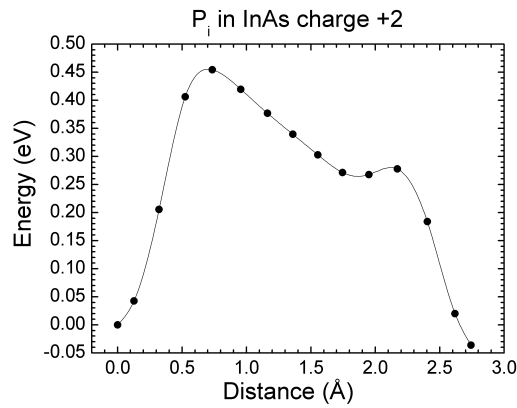


Figure S28. Energy profile for transition of an interstitial P atom in InAs to a substitution position in the As sublattice with the displacement of the As atom into the interstitial position for the +2 charge state $P_i \rightarrow P_{\text{As}} + \text{As}_i$.